BILINGUAL
PUBLISHING CO.
Pioneer of Global Academics Since 1984

01

Journal of Mechanical Engineering Research

Volume 4 Issue 1 · March 2021 · ISSN：2630-4945（Online）

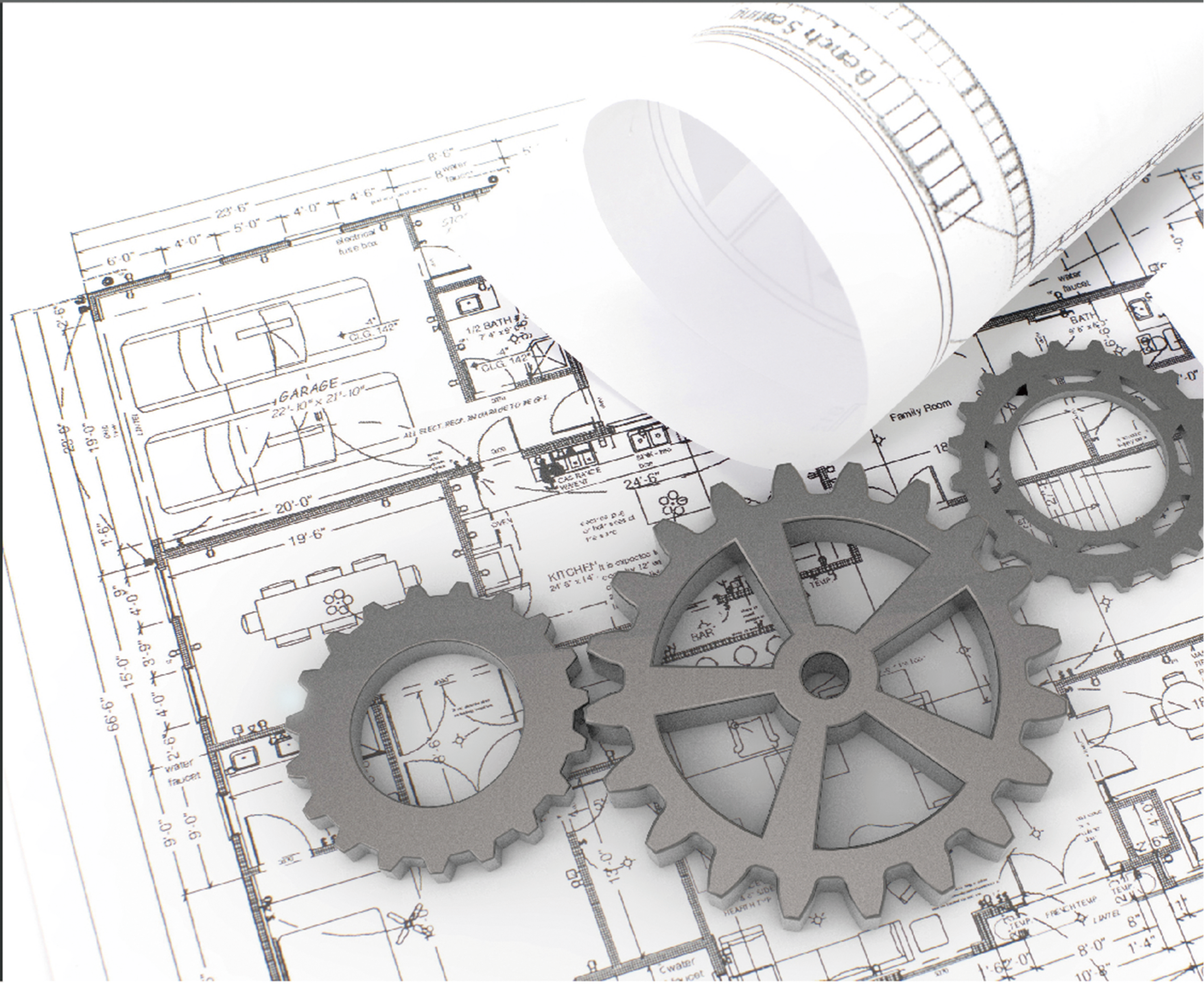

BILINGUAL
PUBLISHING CO.
Pioneer of Global Academics Since 1984

Editor-in-Chief

Dr. Shankar Chakraborty
Jadavpur university, India

Editorial Board Members

Manuel Teixeira Braz-Cesar, Portugal
Gadang Priyotomo, Indonesia
Asit Kumar Parida, India
Ravinder Kumar, India
Milon Selvam Dennison, India
Uziel Yuri Sandler, Israel
Mohaned El wazziki, Canada
Zichen Deng, China
Khalil Ur Rehman, Pakistan
Ravindra Jilte, India
Ramin Kouhikamali, Iran
Satish Kumar, India
Mehdi Safari, Iran
Enock Andrews Duodu, Ghana
Santosh N. Shelke, India
Tso-Liang Teng, Taiwan
Yihua Cao, China
Nan Wu, Canada
Xikun Wang, China
Arash Reza, Iran
Mohammad Nimafar, Iran
Kutsİ Savaş Erduran, Turkey
Xinming Zhang, China
Ashok M Hulagabali, India
Abdelkader Doudou, Morocco
Mousa Khalifa Ahmed, Egypt
Wenbin Wang, China
Daniele Cafolla, Italy
Farshad Abbasi, Iran
Sathyashankara Sharma, India
Ahmet YILDIZ, Turkey
Lyudmila Ivanovna Gracheva, Ukraine
Samuel Filgueiras Rodrigues, Brazil
Samad Nadimi Bavil Oliaei, Turkey
Pravin Tukaram Nitnaware, India
Raj Rani Bhargava, India
Majid Jabbari, Iran
Alper Uysal, Turkey
Arnaldo Casalotti, Italy
Ikram Ullah, Pakistan
Shubhashis Sanyal, India
Matteo Strozzi, Italy
Youliang Huang, China
Vahid Tahmasbi, Iran
Akbar Salemi, Iran
Asim Mukhopadhyay, India
Elammaran Jayamani, Malaysia
Xuejun Jason Liu, United States
Philemon Kazimil Mzee, Tanzania
Amr Kaood, Egypt
Yuan Kang, China
Mohamed Ibrahim Othman, Egypt
Seyed Masoud - Vahedi, Iran
Mohammed Diany, Morocco
Shuang Li, China
Fengxian Xin, China
Ahad - Gholipoor, Iran
Venanzio Giannella, Italy
Hongping Hu, China
Rong Chen, China
Jiusheng Bao, China
Milad Armin, United Kingdom
Yinghong Peng, China
Yu-Chun Kung, United States
Guang Yih Sheu, Taiwan
Siavash Azimi, Iran
Salah Aguib, Algeria
Artur Portela, Brazil
Jun Peng, China
Muhammad - Asif, Pakistan
Ambreen Afsar Khan, Pakistan
Hao Wang, China
Bikash Sahoo, India
Wuyi Wan, China
Hossein Hemmatian, Iran
Fuji Wang, China
Humaira Yasmin, Saudi Arabia
Varinder Kumar Singh, India
Md Muslim Ansari, India
Bing Yang, China
Kuo Liu, China
Ladeesh Vgvg, India
Vinothkumar Sivalingam, India
Saad AbdelHameed EL-Sayed, Egypt
Sedat Yayla, Turkey
Paweł Grzegorz Kossakowski, Poland
Mohamed El-Amine Slimani, Algeria
Mohamed Kamal Ahmed Ali, Egypt
Chew Kuew Wai, Malaysia
Anna Valentinovna Morozova, Russian Federation
Liancun Zheng, China
Bounit Ahmed, Morocco
Kishore Debnath, India
XinJiang Lu, China
Shahriar - Dastjerdi, Iran
Mohamed Nabil Allam, Egypt
Afshin Zeinedini, Iran
Jinglun Fu, China
Rongyun Zhang, China
Pradeep Kumar Gautam, India
Marcos Rodriguez Millan, Spain
Wei Cao, China
Hamdy Mahmoud Youssef, Saudi Arabia
Catalin Iulian Pruncu, United Kingdom
Jan Awrejcewicz, Poland
Nima Ahmadi, Iran
Vipin Nair, India
MD Shamshuddin, India
Reza Aghaei-Togh, Iran
Lie Sun, China

Volume 4 Issue 1 • March 2021 • ISSN 2630-4945(Online)

Journal of Mechanical Engineering Research

Editor-in-Chief

Dr. Shankar Chakraborty

BILINGUAL
PUBLISHING CO.
Pioneer of Global Academics Since 1984

BILINGUAL PUBLISHING CO.
Pioneer of Global Academics Since 1984

Volume 4 | Issue 1 | March 2021 | Page 1-35
Journal of Mechanical Engineering Research

Contents

Article

Journal of Mechanical Engineering Research
http://ojs.bilpublishing.com/index.php/jmer

ARTICLE

Analysis of Turbulence on Cylinder with Additional Fairing with Free Surface

Siqin Chen[1] Xiaomin Li[2*]

1.China University of Petroleum, Beijing, China
2.Yunnan Normal University College of Arts and Sciences, Kunming, China

ARTICLE INFO

Article history
Received: 1 December 2020
Accepted: 27 January 2021
Published Online: 9 April 2021

Keywords:
Numerical simulation
Computational fluid dynamics (CFD)
Volume of fluid
Free surface of liquid

ABSTRACT

In this study, two dimensional unsteady flows of cylinder and cylinder with additional fairing close to a free surface were numerically investigated. The governing momentum equations were solved by using the Semi Implicit Method for Pressure Linked Equations(SIMPLE). The Volume of Fluid(VOF) method applied to simulate a free surface. Non- uniform grid structures were used in the simulation with denser grids near the cylinder. Under the conditions of Reynolds number 150624, 271123, 210874 and 331373, the cylinders were simulated with different depths of invasion. It was shown that the flow characteristics were influenced by submergence depth and Reynolds numbers. When the cylinder close to the free surface, the drag coefficient, lift coefficient and Strouhal numbers will increase due to the effect of free liquid surface on vortex shedding. With additional fairing, can effectively reduce the influence of the free surface on the drag coefficient. Fairing will reduce lift coefficient at high Reynolds numbers, but increase lift coefficient when Reynolds numbers are small. Fairing can effectively reduce Strouhal numbers, thus can well suppress the vortex induced vibration.

1. Introduction

In many ocean engineering, shipbuilding engineering, etc., the phenomenon of fluid pressure and atmosphere communication is widespread. In actual engineering, deep-sea drilling, underwater oil and gas pipelines will all affect the surrounding flow field under the action of free liquid surface. Due to the effect of wind load in the entire field, the phenomenon of air inhalation and bubble collapse of the cylinder in the flow field, the study of the hydrodynamic characteristics of the free surface structure has become one of the research problems. Among them, the flow around a cylinder is one of the classic problems in hydrodynamics.

Researchers have achieved effective results on the problem of flow around a cylinder that ignores the phenomenon of free surface motion under the condition of low Reynolds number, and the related problems of high Reynolds number are still being discussed and studied. In 1961, A. Roshko [1] conducted a flow experiment around a cylinder under a high Reynolds number ($10^6<Re<10^7$) in a wind tunnel, and found that when $Re>3.5\times10^6$, the drag coefficient tends to a constant 0.7 and St is stable at 0.27 In 1964, Hseh obtained the relationship curve of the total resistance coefficient with the Fr number, that is, the resistance value reached the maximum when Fr was approxi-

---

**Corresponding Author:*
Xiaomin Li,
Yunnan Normal University College of Arts and Sciences, Kunming, China;
Email: 2562275375@qq.com

DOI: https://doi.org/10.30564/jmer.v4i1.2643

mately equal to 1. In 1969, Bearman [2] conducted experiments on the vortex shedding phenomenon with Reynolds number in the range of $2\times10^5<\text{Re}<5.5\times10^5$ in the circulating water tank, and measured the resistance, pulsating lift, St and other hydrodynamic parameters under different Reynolds numbers. In 1983, G. Schewe [3] conducted a wind tunnel experiment on the flow around a cylinder in the range of $2.3\times10^4<\text{Re}<7.1\times10^6$ for the Reynolds number, and obtained a steep drop in the drag coefficient and an increase in the Steroha number and other changes.

In 2003, Chaplin and Teigen found that the local resistance near the free surface is reduced. Yu [4], Suh [5], Graf [6], Kawamura [7] and others have carried out related numerical simulation studies, and also proved that when the Re number is less than 1.4×10^5, the drag coefficient at the liquid surface is less than 1.2.

In 2004, Chui-Jie Wu [8] used the dynamic boundary control technology to study the flow around a cylinder and found that the moving wave wall can effectively suppress the separation of the flow vortex around the cylinder and eliminate the oscillation wake. In 2005, Choi [9] found that the distribution of sinusoidal pressure with a specific phase angle in the span direction can significantly reduce the fluctuation of average drag and lift. In 2013, Wu Yucheng [10] studied the influence of the fairing on the flow field. Experimental results show that the fairing can improve the flow field and reduce the fluid resistance of the structure by more than 50%.

In the current research, most of the analysis of flow around a cylinder does not consider the influence of free liquid on its flow. In some pools, due to the small depth of the pool, the pipeline will be closer to the water surface. In this case, the influence of the free surface needs to be considered when analyzing the surrounding flow field. The main purpose of this article is to study the effect of free surface on vortex-Induced vibration and how to eliminate these effects.

2. Numerical Theory

2.1 Governing Equations

The basic governing equations of fluid dynamics include continuity equation, momentum equation and energy conservation equation. In this paper, considering water medium as an incompressible fluid, while air medium had less effect on the results, and it can also be simplified as an ideal gas. Continuity equation and momentum conservation equation should be considered when setting parameters. Continuity equation and momentum conservation equation are given in Equation (1) and Equation (2).

$$\nabla\cdot\mathbf{u}=0 \tag{1}$$

$$\frac{\partial}{\partial t}(\rho\mathbf{u})+\nabla\cdot(\rho\mathbf{u}\otimes\mathbf{u})=\nabla\cdot(\mu\nabla\otimes\mathbf{u})-\nabla P+\rho g \tag{2}$$

u, ρ, P and g represent the velocity vector, fluid density, pressure and gravitational acceleration.

2.2 Turbulence Model

k-ε model with two equations is the most widely used model for viscous flow. This model is further divided into standard *k-ε* model, RNG *k-ε* model and Realizable *k-ε*model.

Standard *k-ε* model assuming that the flow is completely turbulent, the influence of molecular viscosity can be ignored. The model has a wide range of applications and reasonable accuracy, and it is the main tool in engineering flow field calculations. It's formed by new equation of turbulence dissipation rate on the basis of the original single equation model. This model requires the flow field is assumed to be complete turbulence field. In this study, standard *k-ε* model was chosen. Turbulent kinetic energy equation and turbulent dissipation equation are given in Equation (2) and Equation (3).

$$\frac{\partial(\rho k)}{\partial t}+\frac{\partial(\rho k u_i)}{\partial x_i}=\frac{\partial}{\partial x_j}\left[\left(\mu+\frac{\mu_t}{\sigma_k}\right)\frac{\partial k}{\partial x_j}\right]+G_k+G_b-\rho\varepsilon-Y_M+S_k \tag{3}$$

$$\frac{\partial(\rho\varepsilon)}{\partial t}+\frac{\partial(\rho\varepsilon u_i)}{\partial x_i}=\frac{\partial}{\partial x_j}\left[\left(\mu+\frac{\mu_t}{\sigma_\varepsilon}\right)\frac{\partial\varepsilon}{\partial x_j}\right]+C_{1\varepsilon}\frac{\varepsilon}{k}\left(G_k+C_{3\varepsilon}G_b\right)-C_{2\varepsilon}\rho\frac{\varepsilon^2}{k}+S_\varepsilon \tag{4}$$

G_k , G_b represent turbulent kinetic energy due to mean velocity gradient, turbulent kinetic energy due to buoyancy. σ_k and σ_ε represent the turbulence Prandtl number corresponding to k and ε, S_k and S_ε are defined by user, $C_{1\varepsilon}$, $C_{2\varepsilon}$ and $C_{3\varepsilon}$ are empirical constant.

2.3 Flow Parameters

Drag coefficient is a dimensionless number of the effect of momentum transfer to the ground. Lift coefficient is a dimensionless coefficient that relates the lift force generated by a lift to the density of the nearby fluid, the fluid velocity, and the associated reference area. Those are important parameters in fluid flow analysis.

Calculations of the drag and lift coefficients on the cylinder surfaces are given in Equation (5), (6). Drag and lift forces are calculated by the viscous and pressure forces on the surfaces of the cylinders. The formulas are given in

DOI: https://doi.org/10.30564/jmer.v4i1.2643

Equation (7), (8). The Strouhal number is given in Equation (9).

$$CL_{mean} = \frac{2F_L}{\rho U_{\infty}^{2} D} \tag{5}$$

$$CD_{mean} = \frac{2F_D}{\rho U_{\infty}^{2} D} \tag{6}$$

$$F_D = \int_0^D \left(\tau_t(x) + \tau_b(x)\right) dx + \int_0^D \left(P_{f\tau}(y) + P_{\tau}(y)\right) dy \tag{7}$$

$$F_L = \int_0^D \left(\tau_{fr}(y) + \tau_r(y)\right) dy + \int_0^D \left(P_t(x) + P_b(x)\right) dx \tag{8}$$

$$St = \frac{fD}{U_{\infty}} \tag{9}$$

In Equation (7), (8), fr, r, t and b represent the front. back, upper and lower surfaces of cylinders respectively, D represents characteristic length of the structure. In Equation (9), *f* represents the vortex shedding frequency.

2.4 Multiphase Flow Model

The multiphase flow model in fluent has three types: Volume of Fluid Model(VOF model), Mixture model and Euler model. Among them, the VOF model is suitable for dealing with multiphase flow problems that do not intersect each other, such as free surface flow problems. The Mixture model is suitable for the flow analysis of particles in fluids including low powder-carrying airflow and bubble-containing flow. Euler model is suitable for bubble column, casting riser, particle suspension and other problems. In this case, it is more appropriate to choose the VOF model due to the study of free surface flow.

2.4.1 Continuity Equation

Tracking the interface between the phases is accomplished by solving the continuous equation of the volume ratio of one or more phases. For the qth phase, there is:

$$\frac{\partial \alpha_q}{t} + \vec{v} \cdot \alpha_q = \frac{S_{\alpha q}}{\rho_q} \tag{10}$$

Among them: $S_{\alpha q}$ is the mass source term. By default, the source term at the right end of Equation (10) is zero, but when you specify a constant or user-defined mass source for each phase, the right end is not zero. The calculation of the volume fraction of the main phase is based on the following constraints:

$$\sum_{q=1}^{n} \alpha_q = 1 \tag{11}$$

2.4.2 Attribute Calculation

The attributes that appear in the transport equation are determined by the phases that exist in each control volume. Assuming that in a two-phase flow system, the phases are represented by subscripts 1 and 2. If the volume fraction of the second phase is tracked, the density in each unit is as follows:

$$\rho = \alpha_2 \rho_2 +)(1\text{-}\alpha_2 \quad \rho_1 \tag{12}$$

Generally, for an n-phase system, the volume ratio average density takes the following form:

$$\rho = \sum \alpha_q \rho_q \tag{13}$$

2.4.3 Momentum Equation

By solving a single momentum equation in the entire region, the velocity field obtained is shared by each phase. The momentum equation depends on the volume ratio of all phases passing through the properties ρ and μ, and the equation is as follows:

$$\frac{\partial}{\partial t}(\rho \vec{v}) + \nabla \cdot (\rho \vec{v}\vec{v}) = -\nabla p + \left[\mu\left(\nabla \vec{v} + \nabla \vec{v}^{T}\right)\right] + p\vec{g} + \vec{F} \tag{14}$$

2.4.4 Energy Equation

The energy equation is also shared in each phase, expressed as follows:

$$\frac{\partial}{\partial t}(\rho E) + \nabla \cdot \left[\vec{v}(\rho E + p)\right] = \nabla \cdot (k_{eff} \nabla T) + S_h \tag{15}$$

In this equation, k_{eff} is effective thermal conductivity, S_{h} is source terms, including radiation and other volumetric heat sources, *E* is total energy.

2.5 Numerical Details

In order to compare the results with actual test results, the parameters we choose in this study all refer to the parameters used in the actual test.

The cylinder and the computational domain are shown

DOI: https://doi.org/10.30564/jmer.v4i1.2643

in Figure 1, and 2D model was used in this simulation. The diameter of the cylinder(D) was 0.3048m; the distance between free surface and the center of the cylinder(H) was 1D; 2D; 3D; 4D and 5.5D. Cylinder with additional fairing and the computational domain are shown in Figure 2, expect for changing the structure. Other conditions are all same as the cylinder model does.

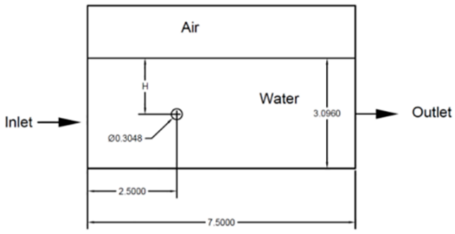

Figure 1. Computational domain for cylinder close to a free surface

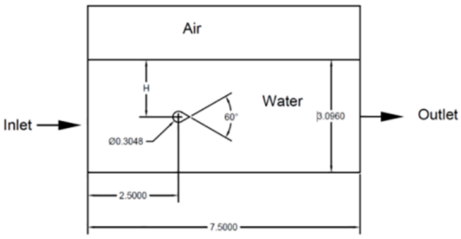

Figure 2. Computational domain for cylinder with additional fairing close to a free surface

A non-uniform grid structure was used, grids around the cylinder and the fairing are presented in Figure 3 and Figure 4.

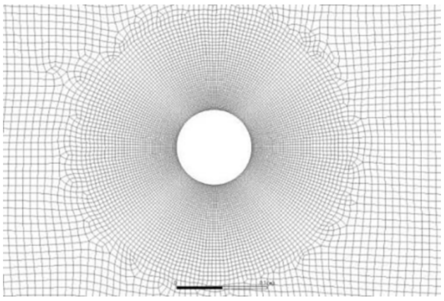

Figure 3. Grid around the cylinder

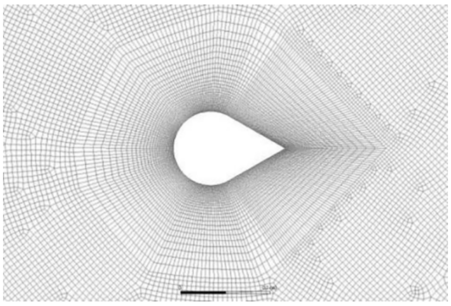

Figure 4. Grid around the cylinder with addition fairing

Simulations were performed at the Reynolds numbers(Re) 150624, 210874, 271123, 331373. Inlet was set as velocity inlet, out let was set as outflow, all boundaries about air were set as symmetry, the structure and the lower boundary were set as wall. Multiphase model chose VOF model and viscous model chose standard *k-ε* model. SIMPLE algorithm is adopted for pressure velocity coupling, Least-Squares Cell Based interpolation algorithm was adopted, transient format was adopted Second order Implicit, pressure difference algorithm was adopted second order format, and momentum difference algorithm was adopted Second order format. All residual accuracy controls were set as 10^{-4}.

Choose the Cd value comparison under the Reynolds number 210874, H/D=5 to check the grid independence, and the results are as follows:

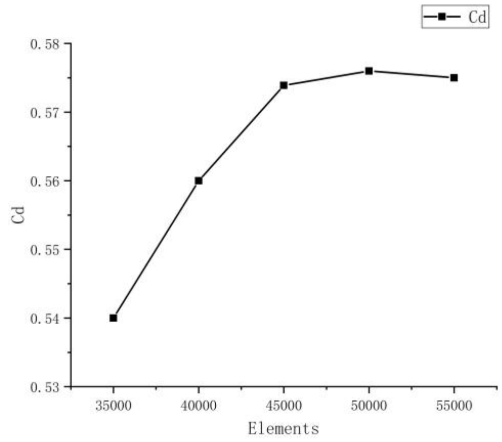

Figure 5(a). The grid dependency tests for cylinder

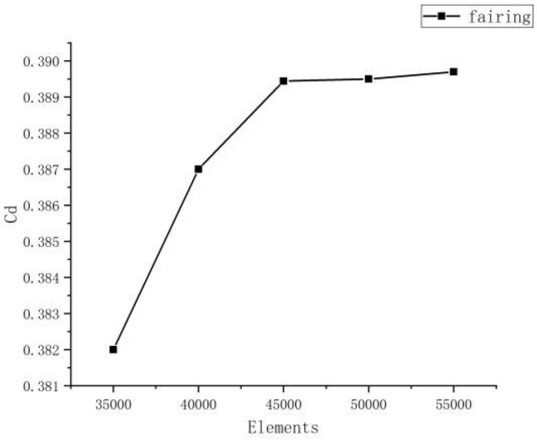

Figure 5(b). The grid dependency tests for fairing

According to the results of the grid independence check, 45,000 elements and 46,000 nodes are selected for simulation

DOI: https://doi.org/10.30564/jmer.v4i1.2643

3. Results and Discussions

2.1 Results of Cylinder

3.1.1 Effect of Submergence Depth

Figure 6 presents the vorticity magnitude at various submergence depth for Re=331373, when H≥2D, the more cylinder close to the free surface, the more vortex shedding becomes intense. One the one hand, because of the influence of free surface, some vortices fall off before they develop into larger size vortices. When H=1D, free surface will affect the formation of vortices, as Figure 6(e) presenting, there are no vortices formed under this condition. On the other hand, it's easy to generate waves when the cylinder close to the free surface and wave will affect vortex shedding.

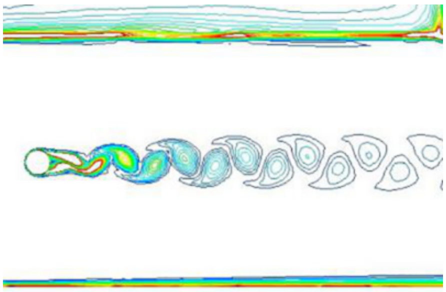

Figure 6(a). Vorticity magnitude of the cylinder for H/D=5

Figure 6(b). Vorticity magnitude of the cylinder for H/D=4

Figure 6(c). Vorticity magnitude of the cylinder for H/D=3

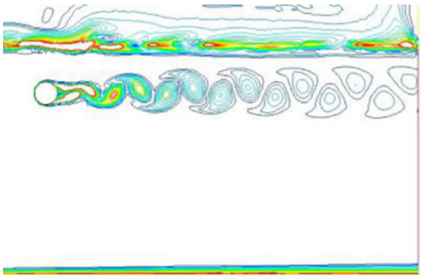

Figure 6(d). Vorticity magnitude of the cylinder for H/D=2

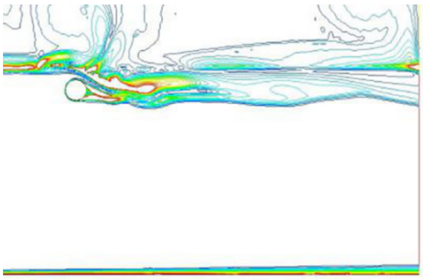

Figure 6(e). Vorticity magnitude of the cylinder for H/D=1

3.1.2 Effect of Reynolds Number

Figure 7 presents the vorticity magnitude at different Reynolds number for H=4D, to clarify the effect of Reynolds number on the vorticity magnitude. As the value of Reynolds number increasing, the size of vortices become more big and the number of vortices increase.

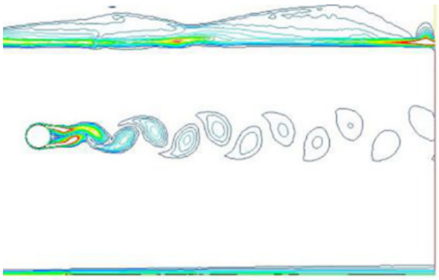

Figure 7(a). Vorticity magnitude of the cylinder for Re=150624

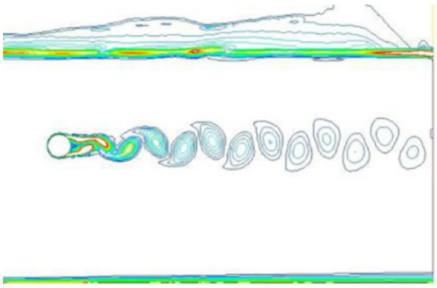

Figure 7(b). Vorticity magnitude of the cylinder for Re=271123

DOI: https://doi.org/10.30564/jmer.v4i1.2643

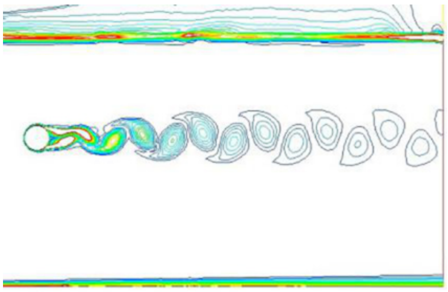

Figure 7(c). Vorticity magnitude of the cylinder for Re= 210874

Figure 7(c). Vorticity magnitude of the cylinder for Re=331373

3.1.3 Results of Flow Parameters on the Cylinder

3.1.3.1 Drag Coefficients

The variation of the mean drag coefficient on the cylinder with submergence depth is present in Figure 8 for different Reynolds number.

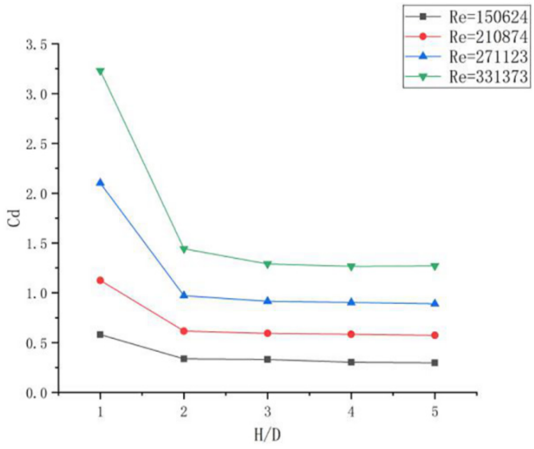

Figure 8. Variation of Cd of cylinder in different Reynolds number

As the H/D increases, the mean drag coefficient on the cylinder becomes smaller at all the Reynolds number. The value of Cd decreases more intense with higher Reynolds number, especially when H/D<3. Because when the cylinder close to the free surface, fluctuation and deformation of free surface will disturb the flow field around the cylinder, thus affect the drag force on the cylinder. When H/D≥3, as submergence depth increases, the influence of free surface becomes smaller.

The mean value of Cd increases as Reynolds number increases at all the submergence depth. Cd will increase sharply if the cylinder is very close to the free surface. As the H/D increase, the growth trend for Cd has slowed.

3.1.3.2 Lift Coefficients

The variation of the root square(RMS) value of lift coefficient on the cylinder with submergence depth is present in Figure 9 for different Reynolds number.

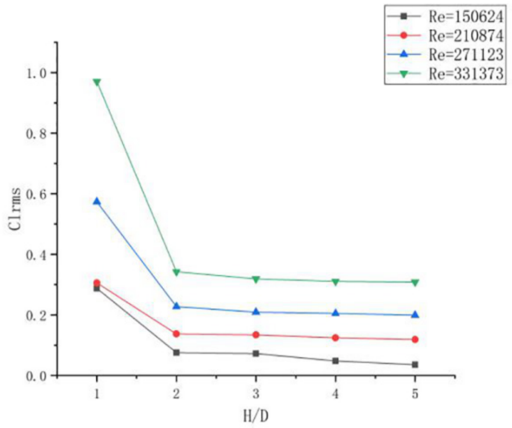

Figure 9. Variation of Cl_{rms} of cylinder in different Reynolds number

The RMS value of lift coefficient will decrease as H/D increase at all the Reynolds number. When H/D<2, Cl_{rms} will decline acutely as H/D become bigger, when H/D≥2, the decline has moderated. Figure 10 clarify the dynamic pressure with different submergence depth for Re=331373. As figure.10(e) clarify, the free surface will have a remarkable influence on the formation of upper cylinder pressure field, thus affect the lift coefficient, even the position of the maximum pressure has changed due to the effect of free surface. Another reason why the free surface will influence lift coefficient, lift force is caused by the pressure increases on the surface of the cylinder when the vortex shed from one side of the cylinder, resulting in the pressure difference in the transverse direction of the cylinder. So lift coefficient will affect by H/D because the free surface will influence vortex shedding.

As Reynolds number increases, the RMS value of Cl increases at all the submergence depth,. Cl_{rms} will increase sharply if the cylinder is very close to the free surface. As the H/D increase, the growth trend becomes slow.

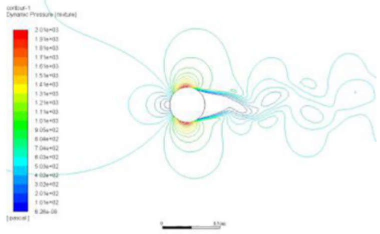

Figure 10(a). Pressure contour of the cylinder for H/D=5

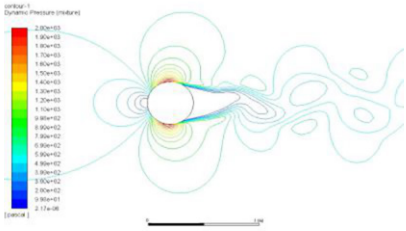

Figure 10(b). Pressure contour of the cylinder for H/D=4

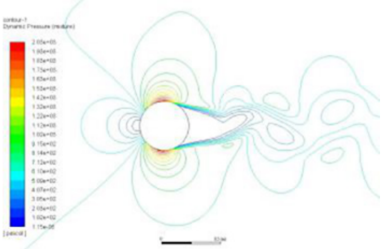

Figure 10(c). Pressure contour of the cylinder for H/D=3

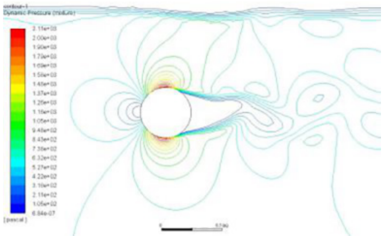

Figure 10(d). Pressure contour of the cylinder for H/D=2

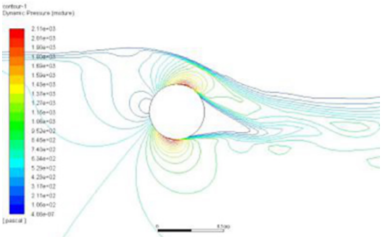

Figure 10(e). Pressure contour of the cylinder for H/D=1

3.1.3.3 Strouhal Number

The variation of St number on the cylinder with submergence depth is present in Figure 11 for different Reynolds number.

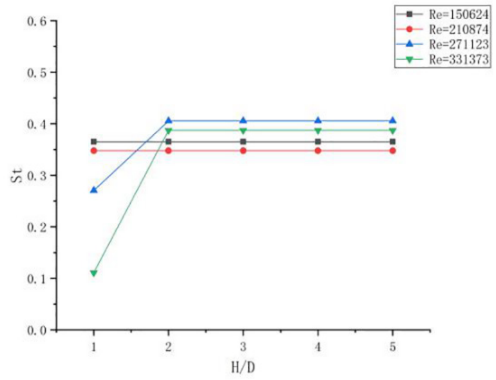

Figure 11. Variation of St of cylinder in different Reynolds number

Strouhal number will not change with submergence depth at Re=150624 and Re=210874. With Re=271123 and Re=331373, Strouhal number will increase first and flatten out when H/D≥2. Between H/D=1 and H/D=2, the higher Reynolds number is, the more drastic the change in Strouhal number. When H/D<2, as the submergence depth increase, the boundary layer thickness on the upper surface of the cylinder increases, the negative and positive vortices shedding become more smoothly. Due to this reason, Strouhal number increases. As the submergence depth increases when H/D≥2, the thickness of the boundaries on the upper and down surface of the cylinder becomes approximately the same, so the Strouhal number will no longer affect by submergence depth. This effect is obvious when the Reynolds number is large.

3.2 Results of Cylinder with Addition Fairing

3.2.1 Effect of Submergence Depth

Figure 12 presents the vorticity magnitude at various submergence depth for Re=331373. With additional fairing, there is no vortex shedding in the wake, so when H/D≥2, the free surface will have little effect on wake. But wake will also damage by waves when the fairing is too close to the free surface.

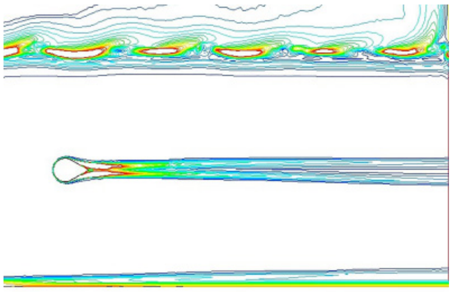

Figure 12(a). Vorticity magnitude of the cylinder with additional fairing for H/D=5

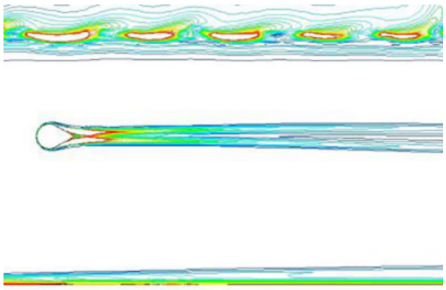

Figure 12(b). Vorticity magnitude of the cylinder with additional fairing for H/D=4

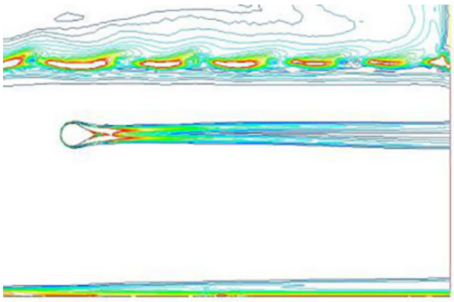

Figure 12(c). Vorticity magnitude of the cylinder with additional fairing for H/D=3

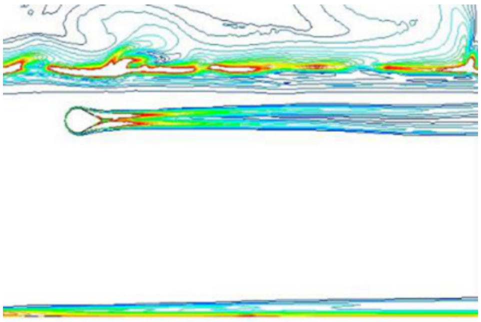

Figure 12(d). Vorticity magnitude of the cylinder with additional fairing for H/D=2

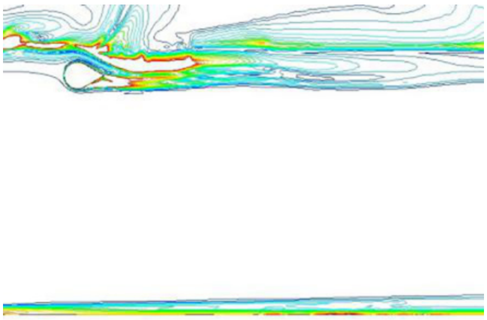

Figure 12(e). Vorticity magnitude of the cylinder with additional fairing for H/D=1

3.2.2 Effect of Reynolds Number

Figure 13 presents the vorticity magnitude at different Reynolds number for H=4D, to clarify the effect of Reynolds number on the vorticity magnitude. When the Reynolds number is small, some small vortices can be observed in the wake. As the Reynolds number increases, the vortices gradually disappear.

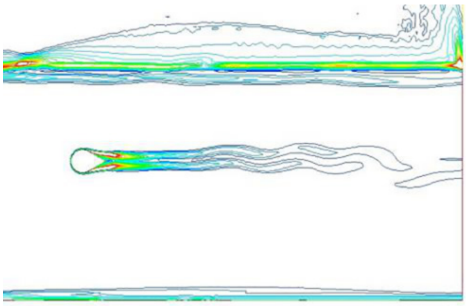

Figure 13(a). Vorticity magnitude of the cylinder for Re=150624

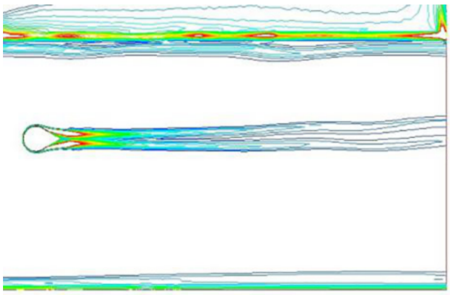

Figure 13(b). Vorticity magnitude of the cylinder for Re=271123

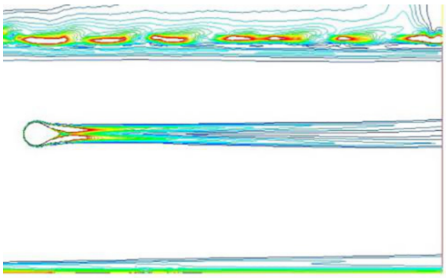

Figure 13(c). Vorticity magnitude of the cylinder for Re=210874

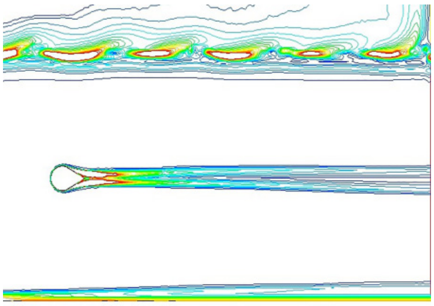

Figure 13(d). Vorticity magnitude of the cylinder for Re=331373

DOI: https://doi.org/10.30564/jmer.v4i1.2643

3.2.3 Results of Flow Parameters on the Cylinder

3.2.3.1 Drag Coefficients

The variation of the mean drag coefficient on the cylinder with additional fairing with submergence depth is present in Figure 14 for different Reynolds number.

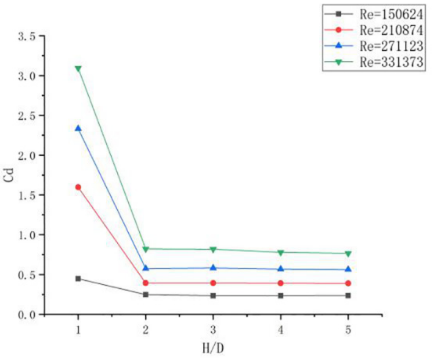

Figure 14. Variation of Cd of cylinder with additional fairing in different Reynolds number

When H/D<2, as value of H/D increases, the Cd will decrease, when H/D≥2, Cd is hardly affected by the H/D value at all Reynolds number. Since there is no vortex shedding in the wake, the effect of the free liquid surface on the Cd value is reduced. However, when the fairing is too close to the free surface, the free surface is severely deformed due to the existence of the fairing, which affects the wake, and has a serious impact on the Cd value. Similar to the situation in the cylinder, the Cd will increase with the increase of the Reynolds number, but compare with Figure 8, the growth trend is obviously slower. It can be seen that fairing can reduce the influence of the free surface to a certain extent, especially when the Reynolds number is low.

3.2.3.2 Lift Coefficients

The variation of the RMS value of lift coefficient on the cylinder with additional fairing with submergence depth is present in Figure 15 for different Reynolds number.

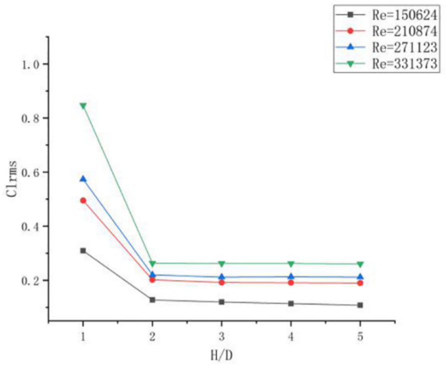

Figure 15. Variation of Cl_{rms} of cylinder in different Reynolds number

When H/D<2, Cl_{rms} will decrease with H/D increases at all Reynolds number.When H/D≥2, Cl has a slight decrease when Re=150624 and Re=21087, remains stable at Re=271123 and Re=331373. At low Reynolds number, the free surface will promote the formation and shedding of vortices, so the Cl_{rms} will decline when submergence depth increase. With big Reynolds numbers, since there are no vortex shedding in the wake, the submergence depth will have limited effect on Cl_{rms}. As Figure 16 clarify, although there is no effect of vortex shedding, the free surface still has a great influence on the pressure field above the fairing, which in turn affects the lift coefficient.

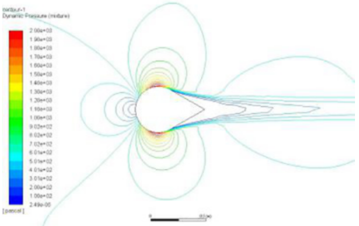

Figure 16(a). Pressure contour of the cylinder with additional fairing for H/D=5

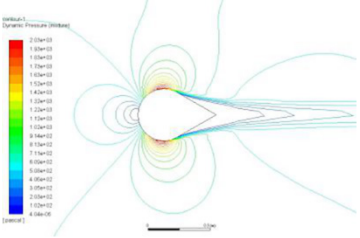

Figure 16(b). Pressure contour of the cylinder with additional fairing for H/D=4

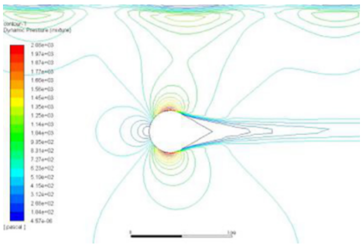

Figure 16(c). Pressure contour of the cylinder with additional fairing for H/D=3

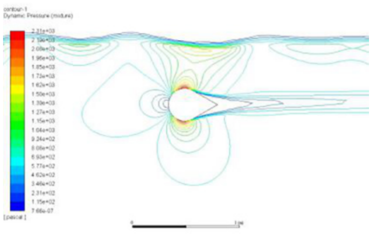

Figure 16(d). Pressure contour of the cylinder with additional fairing for H/D=2

DOI: https://doi.org/10.30564/jmer.v4i1.2643

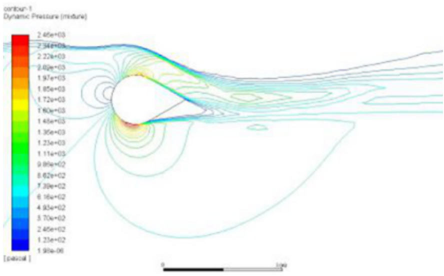

Figure 16(e). Pressure contour of the cylinder with additional fairing for H/D=1

3.2.3.3 Strouhal Number

The variation of St number on the cylinder with additional fairing with submergence depth is present in Figure 17 for different Reynolds number.

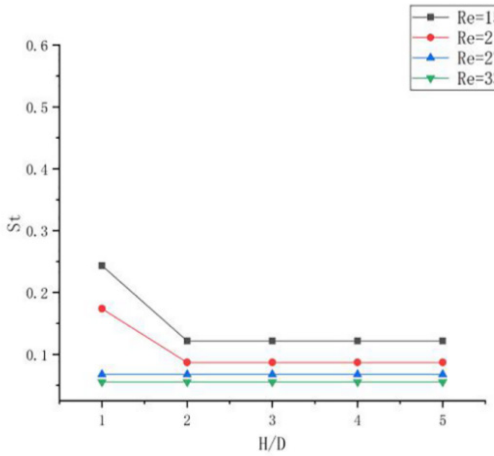

Figure 17. Variation of St of cylinder in different Reynolds number

When the fairing is close to the water surface, at low Reynolds number, the free surface will promote the formation and shedding of vortices, making Stouhal numbers increase. Therefore, for the low Reynolds number, H/D has a greater impact on Strouhal numbers. When H/D<2, the Stouhal numbers will increase as H/D increase. When H/D≥2, as the submergence depth increases, the influence of the free surface decreases and the Strouhal numbers tend to stabilize. At a high Reynolds number, since there are no vortices, it has almost no effect on Strouhal numbers.

3.3 Comparison of the Results of the Two Structures

3.3.1 Drag Coefficient

The variation of the drag coefficient with submergence depth is present in Figure 18 for different structures.

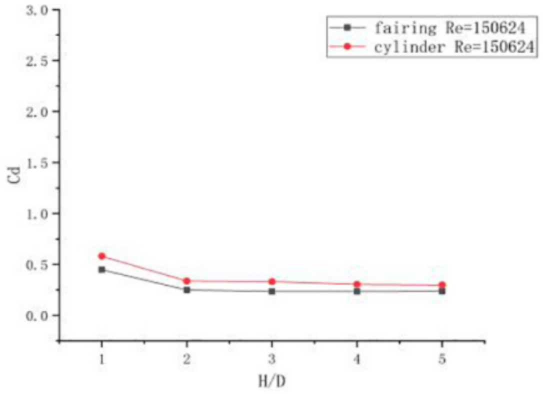

Figure 18(a). Variation of Cd of two different structure in Re=150624

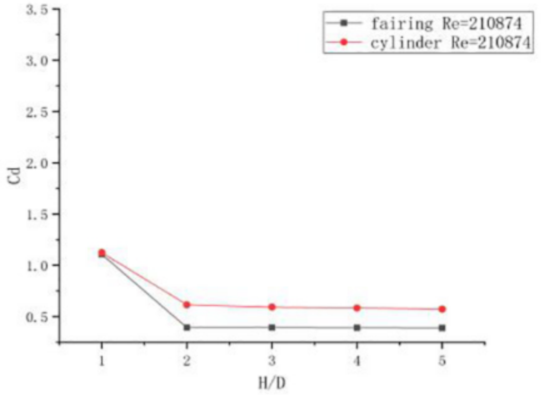

Figure 18(b). Variation of Cd of two different structure in Re=271123

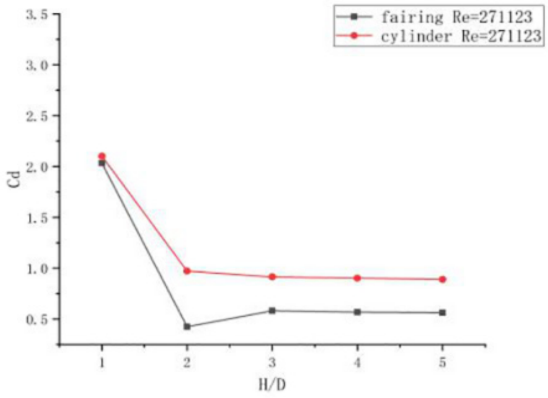

Figure 18(c). Variation of Cd of two different structure in Re=210874

DOI: https://doi.org/10.30564/jmer.v4i1.2643

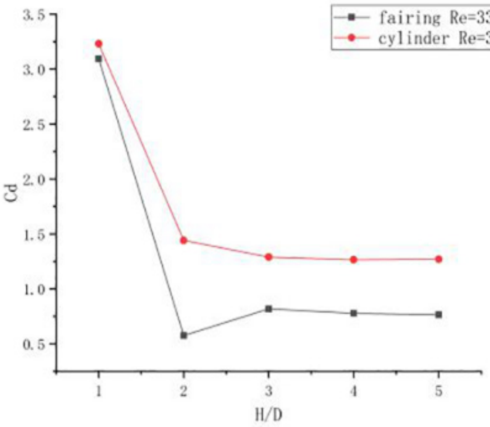

Figure 18(d). Variation of Cd of two different structure in Re=331373

The use of fairing can effectively reduce Cd, and the larger the Reynolds number, the more obvious the effect. The drag force is formed by the pressure difference between the front and back of the cylinder. The larger the Reynolds number, the greater the pressure difference and the greater the drag coefficient. The fairing can effectively reduce the pressure difference between the front and rear of the cylinder, thereby reducing the drag coefficient. But the structure has little effect on Cd when it's too close to the free surface, which is caused by the destruction of the free surface.

3.3.2 Lift Coefficient

The variation of the RMS lift coefficient with submergence depth is present in Figure 19 for different structures.

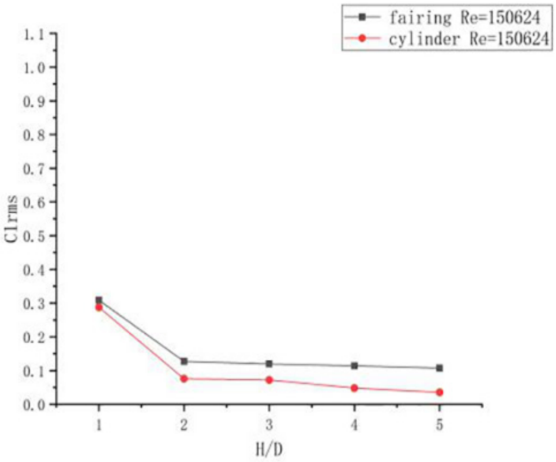

Figure 19(a). Variation of Cl_{rms} of two different structure in Re=150624

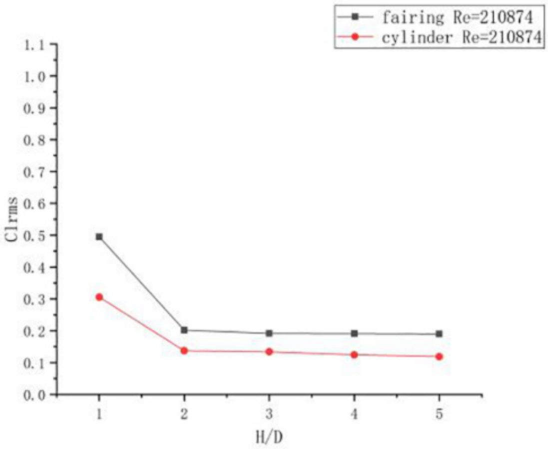

Figure 19(b). Variation of Cl_{rms} of two different structure in Re=271123

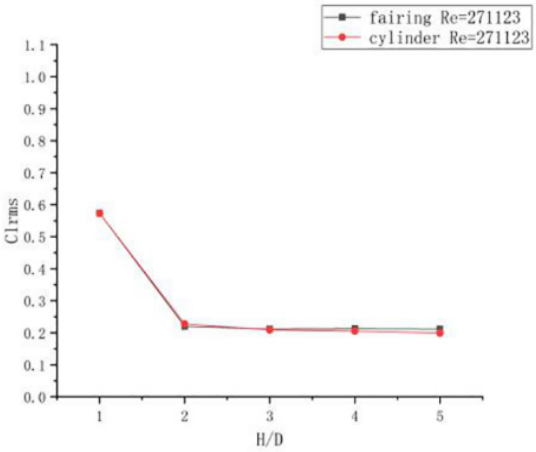

Figure 19(c). Variation of Cl_{rms} of two different structure in Re=210874

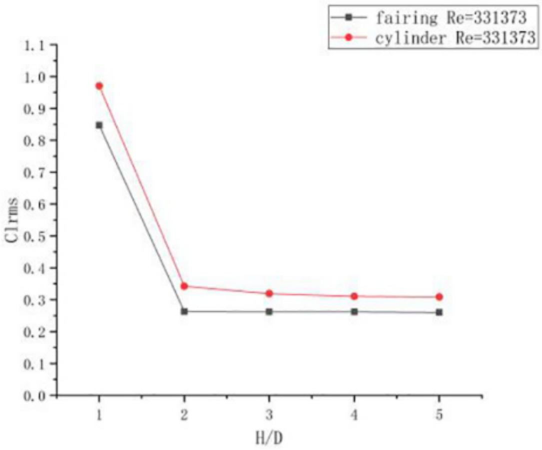

Figure 19(d). Variation of Cl_{rms} of two different structure in Re=331373

At low Reynolds number, the Cl_{rms} of the cylinder is smaller than that of the fairing. When the Reynolds number is low, there is still vortex shedding in the wake of the fairing, and the vortices in the wake are more big and further away from the center line compare with those in cylinder's wake, which cause bigger Cl_{rms}. As the Reynolds number increases, there is no vortex shedding in the wake of the fairing, Cl_{rms} will become smaller than the cylinder at all value of H/D.

3.3.3 Strouhal Number

The variation of the Strouhal number with submergence depth is present in Figure 20 for different structures.

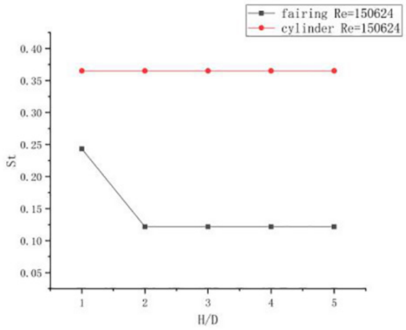

Figure 20(a). Variation of St of two different structure in Re=150624

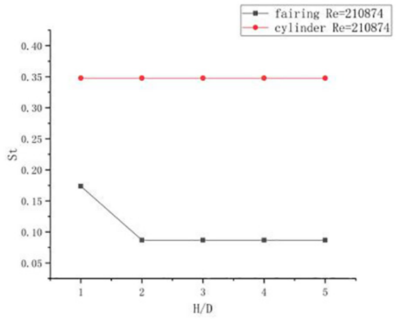

Figure 20(b). Variation of St of two different structure in Re=271123

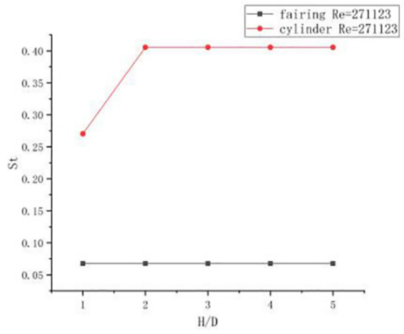

Figure 20(c). Variation of St of two different structure in Re=210874

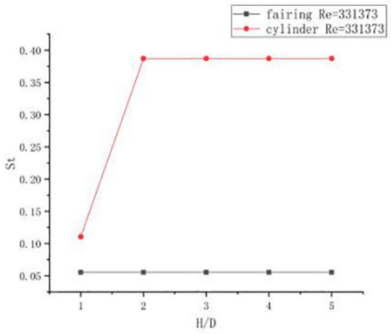

Figure 20(d). Variation of St of two different structure in Re=331373

When the Reynolds number is large, the St value is smaller for cylinder with additional fairing. It indicates that the frequency of vortex shedding is lower under this condition when the Reynolds number and characteristic length are the same. This is because the fairing suppresses the interaction of the shear layers on both sides to a certain extent, thereby suppressing the vortices that alternately shed off. It can be seen that the additional fairing can well suppress the vortex induced vibration. When the Reynolds number is small, part of the vortex remains detached from the wake, and the fairing will increase the St value, indicating that the frequency of vortex shedding is higher under this condition. In general, the value of H/D has little influence on St values of both structures, especially when H/D≥2.

In summary, the existence of the fairing can effectively reduce the Cd value, and effectively reduce the Cl_{rms} value and St value under high Reynolds number, but in the case of low Reynolds number, it will increase the Cl_{rms} value and St value. Therefore, the use of the fairing in the case of high Reynolds number can effectively reduce the drag force and effectively suppress the vortex-Induced vibration.

3. Conclusions

In this study, the flow around cylinder and cylinder with additional fairing placed in a free surface channel was investigated numerically. When the cylinder close to the free surface, the drag coefficient will increase, and the larger the Reynolds number, the more obvious this trend. After attaching the fairing, when H/D≥2, the free surface has a relatively small effect on the drag coefficient, and when the Reynolds number is high, the fairing has a significant effect on reducing the drag coefficient of the cylinder. The lift coefficient will also increase as the cylinder close to the free surface. In the case of high Reynolds number, the additional fairing can reduce the

DOI: https://doi.org/10.30564/jmer.v4i1.2643

lift coefficient, but in the case of low Reynolds number, it will increase the lift coefficient conversely. When the Reynolds number is low, H/D has no obvious effect on the Strouhal number of the cylinder, but under high Reynolds number, when H/D<2, Strouhal number will increase as the increase of H/D, and the larger the Reynolds number , the increasing trend is more obvious. With the addition of the fairing, H/D has a small effect on Strouhal number under high Reynolds number, and has a greater effect under low Reynolds number. The fairing can reduce Strouhal number at all Reynolds number, which can effectively suppress vortex induced vibration. The main reason for these phenomena is that free surface breaks the vortex shedding, with additional fairing, there's less vortex shedding in wake, so the free surface will have influence on drag coefficient and Strouhal number. At low Reynolds number, due to the vortex in the wake, the lift coefficient of the fairing is larger than that of the cylinder. As the Reynolds number increases, the vortex disappears, and the lift coefficient of the fairing is gradually smaller than that of the cylinder.

Data Availability

The data that support the findings of this study are available from the corresponding author upon reasonable request.

References

[1] Schewe G. On the force fluctuations acting on a circular cylinder in cross flow from subcritical up to transcritical Reynolds numbers. J Fluid Mech 1983;133.265–85.

[2] Bearman, P. W. On vortex shedding from a circular cylinder in the critical Reynolds number regime. Journal of Fluid Mechanics, 1969,37(3), 577-585.

[3] Breuer, Michael. A challenging test case for large eddy simulation: high Reynolds number circular cylinder flow. International Journal of Heat and Fluid Flow, 2000, 21.5: 648-654.

[4] Yu D, Kareem A. Numerical simulation of flow around rectangular prism[J]. Journal of wind engineering and industrial aerodynamics, 1997, 67: 195-208.

[5] Suh J, Yang J, Stern F. The effect of air water interface on the vortex shedding from a vertical circular cylinder. ASME J Fluids Eng 2011; 27:1-22.

[6] Graf, W. H., & Yulistiyanto, B. Experiments on flow around a cylinder; the velocity and vorticity fields. Journal of Hydraulic Research, 1998,36(4), 637-654.

[7] Kawamura, T., et al. "Large eddy simulation of a flow past a free surface piercing circular cylinder." Transactions-American Society of Mechanical Engineers Journal of Fluids Engineering.124.1 (2002): 91-101.

[8] Wu, C.J., Wang, L., Wu, J.Z. Suppression of the von Kármán vortex street behind a circular cylinder by a travelling wave generated by a flexible surface. Journal of Fluid Mechanics, 2007, 574, 365-391.

[9] Kim J, Choi H. Distributed Forcing of Flow over a Circular Cylinder[J]. Physics of Fluids, 2005, 17: 033103 1-16.

[10] Wu Yucheng, Wu Shiyuan. ADINA-FSI analysis of vortex induced suppression effect of spiral strake and fairing[J]. China Petroleum and Chemical Standards and Quality, 2013,07:65.

Journal of Mechanical Engineering Research | Volume 04 | Issue 01 | March 2021

BILINGUAL PUBLISHING CO.
Pioneer of Global Academics Since 1984

Journal of Mechanical Engineering Research
http://ojs.bilpublishing.com/index.php/jmer

ARTICLE

Precision Engineering Design Process for Optimal Design Based on Engineering Sciences

Amir Javidinejad*

Boeing Global Services-Engineering Modifications and Maintenance Department, Boeing Company, 4000 N Lakewood Blvd, Long Beach, CA 90846, USA

ARTICLE INFO

Article history
Received: 5 February 2021
Accepted: 23 March 2021
Published Online: 9 April 2021

Keywords:
Optimal design
Good design
Optimization of design
Digitization in design

ABSTRACT

Concepts of precision engineering design process for optimal design where engineering sciences contribute in the successful good design are elaborated in this paper. Scientific theory and practicality are discussed in this paper. Factors necessary for a complete product or systems design are detailed and application of mathematical design optimization in producing a good design are shown. Many applicable engineering design examples are itemized to show relevancy of the optimal design theory to engineering design. Future trends of optimal design with respect to the 4th industrial revolution of digitization are presented. Paper sets to elaborate that most of the engineering and scientific design problems can be optimized to a good design based on many new/advanced optimization techniques.

1. Introduction

To start with, it is essential to understand the classical theories and definitions of “engineering design” and “engineering design process” before moving into the discussion of advanced topics of optimal design based on engineering sciences. According to ABET, engineering design is a process of developing a functional system, component or process to satisfy a series of desired needs and specifications within a defined set of constraints (ABET [1]). Furthermore, ABET states that engineering design “is an iterative, creative, decision-making process in which the basic sciences, mathematics, and engineering sciences are applied to convert resources into solutions. Engineering design involves identifying opportunities, developing requirements, performing analysis and synthesis, generating multiple solutions, evaluating solutions against requirements, considering risks, and making trade- offs, for the purpose of obtaining a high-quality solution under the given circumstances.”

Moving forward to the concept of engineering design process, the process itself is defined by series of process stages known as *research, conceptualization, feasibility assessment, establishing design requirements, preliminary design, detailed design, production planning and tool design, and production* Ertas, A., Jones, J. [2]. Thus, that herby the classical engineering design and engineering design process are defined and clearly made obvious to an engineer; it is necessary to also explore optimal design concept as a fundamental tool. The simplest definition of optimal design is the final set of all known iterative and

---

**Corresponding Author:*
Amir Javidinejad,
Boeing Global Services-Engineering Modifications and Maintenance Department, Boeing Company, 4000 N Lakewood Blvd, Long Beach, CA 90846, USA;
Email: Amir.Javidinejad@gmail.com

DOI: https://doi.org/10.30564/jmer.v4i1.2889

experimental designs that have reached a meaningful statistical definition of best choice that represents the specifications and satisfies the initial and final design constraints.

An optimal design ("Good Design") by definition and by virtue of results is a design where technological factors, user factors and economic feasibility factors come together and produce a complete system or component. Altringer and Habbal [3] indicate that technological factors are based on the engineering, science and math foundations with ergonomics and manufacturing being the common factor with user factors and economic factors, respectively. User factors are based on sociology, psychology and anthropology criteria with marketing being the common factor with the economic factors. Economic feasibility factors are based on the business, market and government criteria. These factors as a whole summarize the requirements for optimal design concepts at a high level that set a preliminary engineering mindset needed for carrying a design process. Refer to Figure 1 for an illustrative purpose of the optimal good design concept.

Other relevant factors that also contribute into a good design are implementation of design thinking with systems thinking for engineering design, Melissa T. Greene, Richard Gonzalez, Panos Y. Papalambros and Anna-Maria McGowan [4]. Melissa Greene [4] elaborate that until recently design thinking and system thinking engineering design were not complimentary to each other. This work by Greene et al. indicated that, in the past, design thinking methods concentrated on industrial design and product development while system thinking engineering design methods was used in professional system engineering practice and large scale, complex designs. This literature [4] indicated that classical design thinking theory, originally introduced by Herbert Simon in 1969, consisted of seven stages for a product design; defining the problem, researching, ideating, prototyping and choosing a solution, implementing the solution and learning. Further, it was indicated by Greene et al., that system thinking engineering design has roots mainly in the operations research where as traditional systems engineering and management science along with dynamic systems, Forrester [5] and General Systems Theory, L. Von Bertalanffy [6] define the system engineering theory. The combination of these two schools of thinking is a modern-day concept for design process where design thinking is required for successful design of products and systems considering all three factors of "good design"; which are technological factors, user factors and economic feasibility factors.

Having established the high-level requirements, scientifically these requirements can be translated into numerical methods established in engineering science theory and practice. Use of numerical methods guarantees the iterations necessary for optimal design approach. CAD and Simulation Tool utilization makes the application of engineering sciences into the design process very lucrative. Good representation of such optimization examples is the structural topology optimizations introduced into civil structural design processes, Georgios Kazakis, Ioannis Kanellopoulos, Stefanos Sotiropoulos and Nikos D. Largaros [7].

For an instance, Georgios Kazakis, Ioannis Kanello-

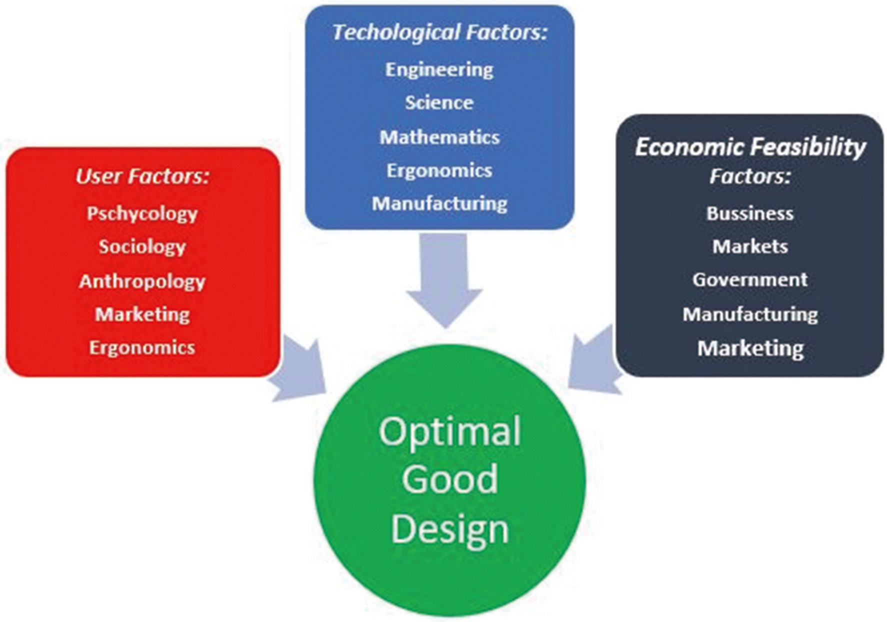

Figure 1. An Optimal Good Design Concept Factors

DOI: https://doi.org/10.30564/jmer.v4i1.2889

poulos, Stefanos Sotiropoulos and Nikos D. Largaros [7], incorporate smart and automated structural computational tools that utilize computational techniques related to topology optimization in civil structural design very logically. The structural topology optimization problem is solved using material distribution methods, L. Spunt [8] for achieving the optimum design layout of a structural system made from linearly elastic isotropic material. For this purpose, a compliance criterion is minimized by adjustment of the material distribution volume into a design domain. The distribution of the material volume in domain is controlled by the density values distributed over the domain. More specifically, it is controlled by design parameters that are represented by the densities assigned to the FE (Finite Element Method) discretization of domain. The FE simulation tool, while under iterative mode, calculates the design variables as the material concentration density is changed. The design variables are limited to strength and displacement outputs that are generated under the applied fixed input loads set at the initiation of the optimization runs. The optimization iteration cycle for an optimally good design is shown in Figure 2 following. Geometry of a product or a system is simulated and material mechanical property definitions are set. Constraint sets are established to define the displacement and strength limits. Once the design analysis is initiated a limit comparison is made against the constraint sets. Material concentration densities are adjusted and once again limit comparisons against the constraint sets are made. Determination of "good design" based on the criterion are made. Iteration process is started until an "optimal" good design is achieved.

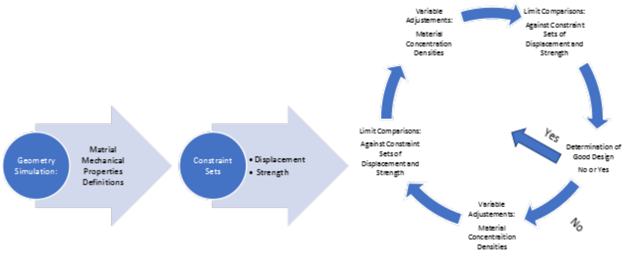

Figure 2. Automatic Optimization Iterations for an Optimal Good Design

The aforementioned research work was mentioned to explore the numerical method aspects of optimal design in a design process via engineering sciences. It is next necessary to explore the user factors in optimal design. It was stated earlier that psychology and sociology are the user factor criterion for design. This is where ergonomics and marketability of the design have to be considered in an optimal design. A design "must" be ergonomically ideal for the user and the design engineer must give maximum considerations for user comfort and safety. The engineering mindset that considers the comfort and safety of the end user always has the best features embedded in the system design or in the component design by definition. Designing for safety by definition has the safety factors embedded in design and any malfunctions are minimized as the design safety is accomplished. In some instances, fail-safe conditions are also a component of the safe design, where as possible failure of the subcomponents of the system does not necessarily indicate a catastrophic failure but rather a controlled failure. These factors in combination with other factors are normally driven by the governmental factors/requirements.

Leading to the final stages of the "good design", economic factors that are based on market, business and government criterion are the most important factors in a good optimal design. For instance, in the telecommunication industry an optimal design considers all applicable IEEE standards which constitute the business standards of the best design process practice. In civil structure designs, in mechanical and aerospace designs ASTM standards for material characterization are standards of the best design process practice for use of material properties. As another example, in automotive engineering SAE standards are criterion that are used for best business standards and practices. Government regulations as set by organizations such as National Highway Traffic Safety Administration (NHTSA), Federal Aviation Administration (FAA) and Individual State and Municipality Building Code Administrations are some of the good examples for a good optimal design requirements.

2. Benefits of Design Optimization for an Optimal Good Design

Historically, design variations done by engineers were limited to shape optimization as a whole with one or two cumbersome iterations only. Automatic design optimizations via computational simulation methods introduced topological optimizations that varied design topology and saved material costs and weight. The concept of varying material density concentration on a system or a part component design as a specific example was unknown and unfeasible in the past. For instance, an airplane part could only be designed with the outside dimensional boundaries varying in an iteration or two. The concept of material concentration density adjustment was unfeasible and far out to reach concept in early days. Computational tools such as FEA (Finite Element Analysis) provided the

DOI: https://doi.org/10.30564/jmer.v4i1.2889

means for such automatic optimization schemes because design variables now can be parametrized and change in them was feasible and not time consuming thus making such optimization efforts possible and reachable. The general application of FEA for optimal design is illustrated in Figure 3 following.

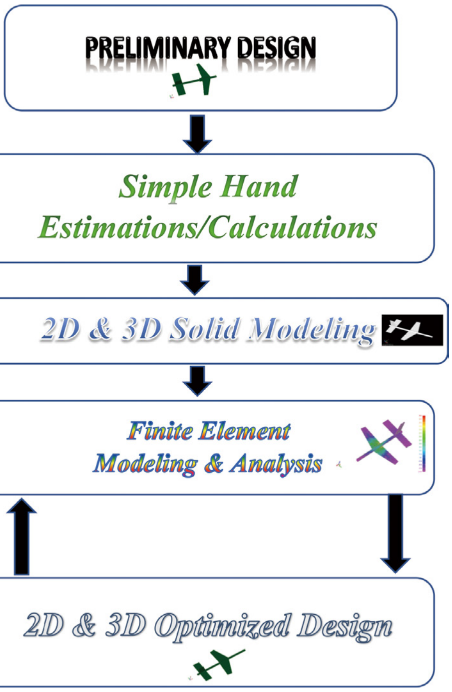

Figure 3. FEA Application for Design Iterations

3. Mathematical Optimization Theory Behind (Numerical Methods)

The best means of defining optimization theory in design is by defining the mathematical concept of the optimization. Mathematical Optimization as defined by J. Snyman [9], is a formal process of formulation and the solution of a constrained problem of the general form.

$$\text{Minimize } f(x),\ x = [x_1, x_2,.., x_n]^T \in R^n \tag{1}$$

w.r.t: x

Subject to constraints:

$$g_j(x) \le 0,\ j = 1, 2, \ \ldots\ , m \tag{2}$$

$$h_j(x) = 0,\ j = 1, 2, \ \ldots\ , r \tag{3}$$

Where $f(x)$, $g_j(x)$ and $h_j(x)$ are scalar functions of the real *column vector* x. The continuous components x_i of $x = [x_1, x_2, \ldots\ ,x_n]^T$ are called the (*design*) *variables*, $f(x)$ is the *objective function*, $g_j(x)$ denotes the respective *inequality constraint functions and* $h_j(x)$ the *equality constraint functions*.

The optimum vector x that solves problems (1) and (2) is denoted by x^* with corresponding optimum function value $f(x^*)$. Mathematically if no constraint sets are specified, the problem is called an *unconstrained* minimization problem.

The iterative means of reaching the solution by minimization optimum function are done by numerical and computational methods; as an example of such cycle was provided with Figure 2 illustrations before.

In general optimization can take effect by means of shape, size or topology, Il Yong Kim, Byung Man Kwak [16], Raino A.E. Makinen, Jacques Periaux and Jari Toivanen [17], C. Onwabiko [18]. There are two main methods for achieving an optimization. One method is the gradient-based method and the other method is Heuristic method. For gradient based method minimization is done based on a function that could hold constraints or be unconstrained. The method tests for convergence of the solution function and if no optimal design is achieved a search in the domain space is done by updating the design variables until a desired optimal design solution is reached, C Onwabiko [18].

Heuristic methods are computational procedures that find an optimal solution by iterative means that improve on sample solution with respect to a given measure of quality. It is randomization of the solution with implementation of genetic algorithms, simulated annealing or tabu search method, Wang, F.S., Chen, L.H. [19].

4. Optimization Design Theory Applicability

The applicability of automatic optimization design theory here in this presentation is somewhat constrained to a specific example of structural optimization. However, the mathematical model can be applicable to any engineering design concept optimization. Likewise, the same theory can be applied to a heat exchanger design concept whereas optimal pipe sizing and pipe count are the objectives of a good design, Bahri Sahin, Yasin Ust, Ismail Teke and Hasan H. Erdem [10]. In this type of research the objective function is defined as the actual heat transfer rate per unit total cost considering lost energy and investment costs. The optimal performance and design parameters which maximize the objective function are investigated with the effects of varying technical and economical parameters. Figure 4 following attempts to illustrate a quasi-realistic typical design optimization effort. As the number of iterations go up the cost has to come down and an optimal design has to be reached all at the same time. This representation is fictional for illustrative purposes and only represents a first pass iter-

DOI: https://doi.org/10.30564/jmer.v4i1.2889

ation segment cut of the optimization theory objective. In reality, this iteration could be chaotic or non-chaotic depending on the sensitivity required for convergence.

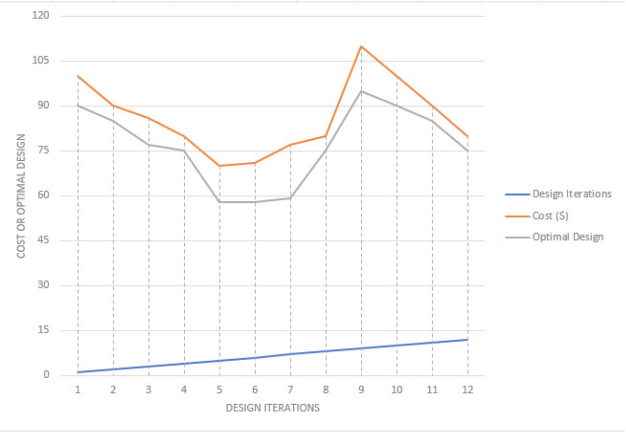

Figure 4. Design Optimization Theory Objective

For illustration purposes let's assume a simple part as shown by the Figure 5 following. This is a part model represented in a CAD model with the illustrated dimensions. One can discretize the model with finite element representation of the model as shown by Figure 6 following. An applied load of 100 pounds is applied to the tip of the part and the part is being held fixed on the other end as shown in Figure 6. The Figure 7 illustrates the first run FEM model with the highest stress level to be around 17ksi. There are many regions within the part design that have very small magnitude of stress concentration level. After the trim and geometric optimization of the external boundary of the part, the second run of FEM analysis is performed. At the second run after optimization based on the stress concentration locations shown the highest stress levels are around 64ksi with about 3% weight reduction. The third and final run the highest stress level is around 79ksi with about 30% weight reduction with the part structural region. The total processing time for this typical part optimization was about 60 minutes to perform a 30% weight reduction.

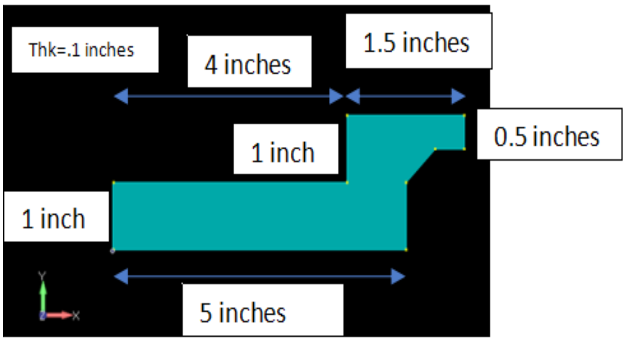

Figure 5. CAD Model of a Part

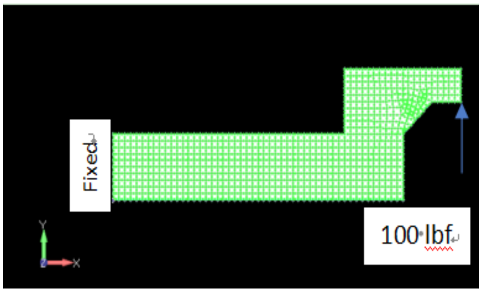

Figure 6. Discretized FEM Model of the Part with BC's

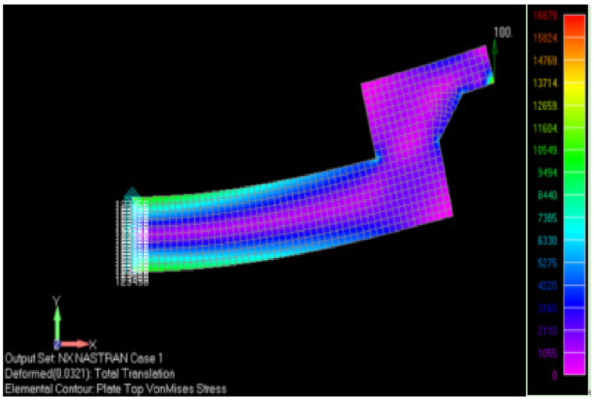

Figure 7. First run of the FEM with the 100 lbs load at the tip

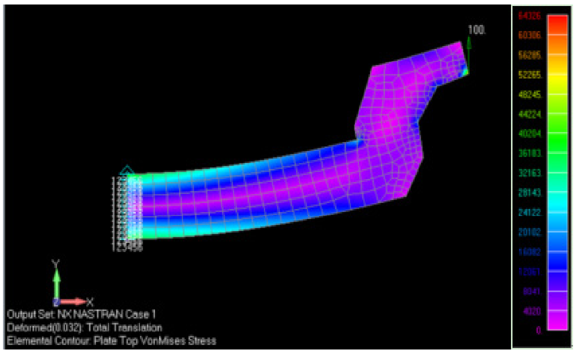

Figure 8. First Run Optimization of the FEM Model (3% weight reduction)

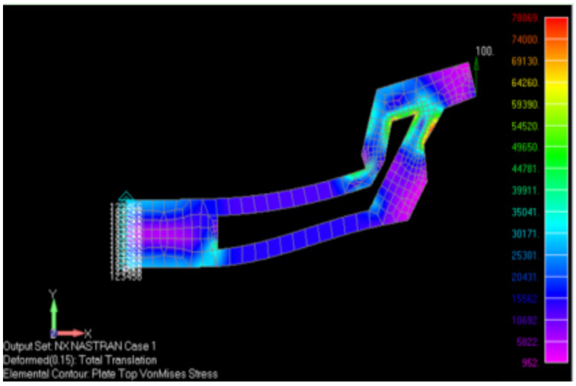

Figure 9. Second Run Optimization of the FEM Model (30% weight reduction)

DOI: https://doi.org/10.30564/jmer.v4i1.2889

In a manufacturing environment, technical and economical parameters are also a design factor for an optimal good design; the same optimization theory is applicable as well too. In a study done by Cezarina, Afteni and Gabriel Frumuşanu [11], a systematic analysis of already published works on formulating and solving optimization problems concerning manufacturing process are presented. The review work done by Cezarina, Afteni and Gabreil Frumuşanu [11] indicate optimization was performed on two levels, namely: planning and scheduling of manufacturing process. Mono-criterion or multi-criteria type of optimization with objective functions set as the energy consumption, the manufacturing costs, the productivity and the manufactured surface roughness were considered. Interestingly, Genetic Algorithms (GA), Particle Swarm Optimization (PSO) technique and Artificial Neural Networks (ANN) are among the methods reviewed for optimization (GA utilization is considered another advanced mathematical theory of optimization).

Furthermore, an advanced improved optimization theory applicable to aircraft sizing problem has been examined by Li, Wei; Xiao, Mi and Gao, Liang [12]. An optimization method is introduced by the authors where three subsystems, aerodynamics, weight and performance are considered. The objective of this optimization is to minimize the total weight of aircraft subject to constraints on the aircraft range and stall speed of the aircraft. This work is indicative that the robustness of the objective and constraints functions simultaneously should be considered for construction of a robustness discrepancy that guides the optimization sampling problem. At first initial feasible solutions are used to build this robustness discrepancy. In detail a set of uncertain candidates that have smaller robustness discrepancy values are selected that meet the robustness requirements. Then a method known as MPS method is used as a global optimizer to achieve the optimal solution. Finally, a sampling method known as ICPM is utilized to address the optimization problem with uncertainties where it is carried out by 9 discrete mathematical steps that are explained in this research work by Li, Wei et al. These types of multidisciplinary robust design optimization methods gain more and more applications in research, Wang X, Wang R, Chen X and Geng X [13] and Zaman K, Mahadevan S [14], where complex design problems with large uncertainties exists.

5. Concepts of Optimal Good Design for the Future

With the new industrial revolution of digitization taking form recently, the good design theory is achieving new levels of complexity and outcome [22]. Not only a good design would be optimized locally at the engineer's simulation level but also it will be optimized and processed via multiple end users and functional inputs. A typical design can have inputs from manufacturing and fabrication facilities, installation and modification sites, marketing inputs, industrial design branch and finally but not least the end user-customer [23].

Decentralizing the decision-making process and information transparency are the main factors of digitization era in design concepts that drive the optimal design in the future. The power of advanced next generation data networks along side with digitization efforts and rendering provide these optimal designs in matter of hours if not minutes depending on the complexity of the problem at hand. Ease of access to design data and design data always being accessible is another advantage of digitization being incorporated into the design process. This concept minimizes the wait time to review and update any design as it allows simultaneous access of design by different people who are involved.

Knowing all that, to progress in this 4th industrial revolution era, understanding classical design optimization theory and application of it, is a must to know venture. Design engineers should not neglect the need to fully understand the classical design optimization theories in order to move forward or at least prove not to be inefficient in the future as the digitization revolution sets in place.

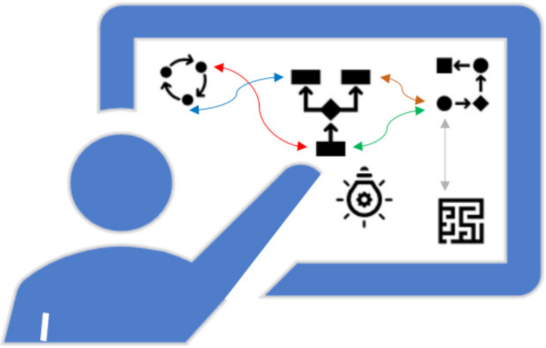

Figure 10. Concepts of Optimal Design for the Future

6. Multidisciplinary Nature of Design

Unlike the early eras of technology development in the world whereas a design was only carried out by one "design engineer" who had basic knowledge of every related field for the design, in this age the designs are 99%

DOI: https://doi.org/10.30564/jmer.v4i1.2889

multidisciplinary efforts. In fact, if different subject matter expert engineers are not involved in the design process, the design is destined to be an average design if not a substandard design for certain. The need for reduction of cost by utilization of advanced materials, materials processes and fabrication techniques requires multidisciplinary expertise for a "good design". The technology has advanced so much and so rapidly that for sure one engineer is not capable of having the full knowledge to carry a "good design" solely by relying on himself or herself alone without other engineers in other disciplines.

7. Discussion

This paper tries to elaborate that most of the engineering and scientific design problems can be optimized for a good design based on many new optimization techniques discussed here. The work presented in this paper implies that there are many factors associated with a good design and further there are a vast variety of optimization techniques that exist in achieving the good design. The user factors, technological and financial feasibility factors that are known, have to be considered in any design problem. Each factor has to be given a real value and each value has to be scaled in the order of the importance. Based on these factors, the parameters for the optimization have to be set and each of the factors has to be translated into design variables and state variables in a scientific manner. The survey of design optimization applications that are sampled in this paper are indicative that there are many numerical and scientific methods in achieving an optimal good design. Thus, depending on the complexity and the degree of uncertainties associated with the design, the optimization can be formulated literally in math models that materialize the robust optimization goals that take away the randomness. It needs to be added that a solid background in mathematical and numerical modeling is a must for achieving a good engineering design [20, 21].

8. Conclusions

The concepts of the good design and optimal good design theory were examined here in this paper. Factors associated with a good design concept; Technological factors, user factors and economic factors were defined and established as tools for a good design concept. Design thinking and system engineering design thinking were elaborated. Design optimization theory with several practical applications in civil structures design, heat exchanger design and manufacturing operation design was discussed in details. The general mathematical theory of optimization was introduced and its application to any design process was emphasized. Future trends of design optimization for a good design in the new era of digitization revolution was discussed and the design engineer's need to familiarize oneself with the classical design optimization theory was emphasized.

References

[1] Accreditation Board of Engineering and Technology (2020), Criteria for Accrediting Engineering Programs-2019-2020, http://www.abet.org/accreditation/accreditation-criteria/criteria-for-accrediting-engineering-programs-2019-2020/#GC5

[2] Ertas, A. & Jones, J. (1996), The Engineering Design Process. 2nd ed. John Wiley & Sons, Inc., New York, N.Y.

[3] Altringer, B., & Habbal, F. (2015), Embedding Design Thinking in a Multidisciplinary Engineering Curriculum. In National Collegiate Inventors and Innovators Alliance (pp. 1–13). Hadley, Massachusetts. Retrieved from http://search.proquest.com/docview/1749280842?accountid=14701\nhttp://sfx.scholarsportal.info/ottawa?url_ver=Z39.88-2004&rft_val_fmt=info:ofi/fmt:kev:mtx:journal&genre=article&sid=ProQ:ProQ:entrepreneurship&atitle=EMBEDDING+DESIGN+THINKING+IN+A+MULTIDISC--

[4] Melissa T. Greene, Richard Gonzales, Panos Y. Papalambros and Anna-Maria McGowan (2017), Design Thinking vs. System Thinking for Engineering Designs: What's the difference, 21st International Conference on Engineering Design, Vancouver, Canada.

[5] Forrester, Jay. (1994), System Dynamics, Systems Thinking and Soft OR, System Dynamics Review, Vol. 10(2) pp. 1-14.
DOI: https://doi.org/10.1002/sdr.4260100211

[6] Ludwig Von Bertalanffy (1940), An Outline of General Systems Theory, British Journal for the Philosophy of Science, Vol. 1 (2) pp. 134-165.
DOI: https://doi.org/10.1177/053901846700600610

[7] Georgios Kazakis, Ioannis Kanellopoulos, Stefanos Sotiropoulos, Nikos D. Lagaros (2017), Topology optimization aided structural design: Interpretation, computational aspects and 3D printing. Heliyon, Vol. 3 e00431.
DOI: https://doi.org/10.1016/j.heliyon.2017.e00431

[8] L. Spunt (1971), Optimum Structural Design, Prentice-Hall, Englewood Cliffs, New Jersey, USA.

[9] Jan N. Snyman (2005), Practical Mathematical Optimization, Springer Science+Business Media, Inc.

[10] Bahri Sahin, Yasin Ust, Ismail Teke and Hasan Huseyin Erdem (2010), Performance analysis and opti-

DOI: https://doi.org/10.30564/jmer.v4i1.2889

mization of heat exchangers: a new thermoeconomic approach, Journal of Applied Thermal Engineering, Vol. 30, Issues 2–3, pp. 104-109.
DOI: https://doi.org/10.1016/j.applthermaleng.2009.07.004

[11] Cezarina, Afteni and Frumuşanu, Gabriel (2017) A Review on Optimization of Manufacturing Process Performance, International Journal of Modeling and Optimization, Vol. 7(3): 139-144.
DOI: https://doi.org/10.7763/IJMO.2017.V7.573

[12] Wei Li, Mi Xiao and Liang Gao (2019), Improved Collaboration Pursing Method for Multidisciplinary Robust Design Optimization, Structural and Multidisciplinary Optimization Journal, pp. 1949-1968.
DOI: https://doi.org/10.1007/s00158-018-2165-2

[13] Wang X, Wang R, Chen X and Geng X (2018), An efficient single loop strategy for reliability-based multidisciplinary design optimization under non-probabilistic set theory, Aerospace Science Technology, Vol. 73: 148-163. https://doi.org/10.1016/j.ast.2017.11.046.

[14] Zaman K and Mahadevan S (2013), Robustness-based design optimization of multidisciplinary system under epistemic uncertainty, American Institute of Aeronautics and Astronautics Journal Vol. 51(5): 1021-1031.
DOI: https://doi.org/10.2514/1.J051372

[15] Martin O. Bendose and N Kikuchi (1988), Generating Optimal topologies in structural design using a homogenization method, Journal of Computational Method Appl Mech Engr, Vol. 71: 197-224.
DOI: http://dx.doi.org/10.1016/0045-7825(88)90086-2

[16] Il Yong Kim and Byung Man Kwak (2002), Design Space Optimization using a Numerical Design Continuation Method, International Journal for Numerical Methods in Engineering, Vol. 53: 1979-2002.
DOI: http://dx.doi.org/10.1002/nme.369

[17] Raino A.E. Makinen, Jacques Periaux and Jari Toivanen (1999), Multidisciplinary Shape Optimization in Aerodynamics, electromagnetics using genetic algorithms, Int Journal for Numerical Methods in Fluid, Vol. 30: 149-159.
DOI: https://doi.org/10.1002/(SICI)1097-0363(19990530)30:2<149::AID-FLD829>3.0.CO;2-B

[18] C. Onwabiko (2000), Introduction to Engineering Design Optimization, Prentice Hall, U.S.A.

[19] Wang, F.S., Chen, L.H. (2013), Heuristic Optimization, Encyclopedia of Biology Systems, Springer, New York NY.

[20] Pahl, G., Beitz, W., Feldhusen, J. and Grote, K-H. (2007), Engineering Design: A Systematic Approach, Springer, New York NY.

[21] Pugh, S. (1991), Total Design: Integration Methods for Successful Product Engineering, University of Michigan, Ann Arbor, Michigan.

[22] Company Blog, (2019), How digitalisation is changing the world of engineering, Item Industrietechnik GmbH, Germany.

[23] Zhou, J., (2013), Digitalization and intelligentization of manufacturing industry. Adv. Manuf. 1, 1-7.

BILINGUAL PUBLISHING CO.
Pioneer of Global Academics Since 1984

Journal of Mechanical Engineering Research
http://ojs.bilpublishing.com/index.php/jmer

ARTICLE

Arc Stability Characterization of Double Coated Electrodes for Hardfacing

Odonel González-Cabrera[1*] Carlos R. Gómez-Pérez[2] HéctorA.Kairús-Hernández-Díaz[3] Félix A. Díaz-Rosell[4]

1.Villa Clara Information and Technological Management Center. Marta Abreu #55 entre Zayas y Villuendas. Santa Clara. Villa Clara.
2.WeldingResearch Center. Central University "Marta Abreu" of Las Villas. Carretera a Camajuaní, km 5 ½. Santa Clara. Villa Clara.
3.Electrical Engineering. Central University "Marta Abreu" of Las Villas. Carretera a Camajuaní, km 5 ½. Santa Clara. Villa Clara.
4.Physics, Mathematics and Computing. Central University "Marta Abreu" of Las Villas. Carretera a Camajuaní, km 5 ½. Santa Clara. Villa Clara.

ARTICLE INFO

Article history
Received: 5 February 2021
Accepted: 31 March 2021
Published Online: 9 April 2021

Keywords:
Arc stability
Welding electrode
Hardfacing
Position of alloy charge

ABSTRACT

The aim of this work is to establish the influence of the relative position of the alloy charge C-Cr-Mn in the structure of the coating of rutile electrodes for hardfacing, on the operational behavior (arc stability). For this, three variants of electrodes with similar chemical composition are elaborated in the metallic core and the coating, differentiating only in the relative position that occupies the alloy charge (C-Cr-Mn) in the structure of the coating: internal, external and homogeneous. For the development of the research, a completely random design is used. The operative characterization of the electrodes is performed in terms of the arc stability. In conclusion, it can be seen that the position of the alloy load influences the operation behavior (stability of the arc). The variant of internal alloy charge in the coating presents the better arc stability performance.

1. Introduction

The evolution of the use of arc welding processes in recent years is well known [1]. In Latin American countries this trend has been less marked, being used for 40% of the metal deposited in countries such as Argentina. In China and India, accompanying the remarkable growth of steel production, there has been a marked increase in the use of coated electrodes. Everything seems to indicate that the use of coated electrodes will stabilize around 30% of the weld metal deposited worldwide [2].

Wear is part of the production process, since metals suffer the effects of abrasive particles that cause sensitive losses in them. The action of these particles in the wear mechanism depends on multiple factors, in addition to the characteristics of the worn material. Research on new materials for hard facing is one of the fields of greatest potential to face phenomena such as the wear of parts and components [3, 4].

**Corresponding Author:*
Odonel González-Cabrera,
Villa Clara Information and Technological Management Center. Marta Abreu #55 entre Zayas y Villuendas. Santa Clara. Villa Clara;
E-mail: ogonzalez@ciget.vcl.cu

DOI: https://doi.org/10.30564/jmer.v4i1.2890

The proper study of the mechanisms of wear contributes in great percentage to make the selection of the appropriate consumable. In some cases, the piece may be subject to several factors. There is no consumable that resists all the previous conditions, but, in practice, an appropriate solution can always be found [5].

Among the factors to be considered in the material deposited to deal with abrasive wear is the hardness of the phases that compose it separately, although this is a much more complex problem. In fact, the hardness is not always the only parameter to take into account in the wear resistance. For example, for the same hardness values of the metal, in martensite and other martensite and carbide compositions, the second will have more wear resistance [6].

The use of welding for hard facing offers unique advantages over other systems for these purposes; a metallurgical union that is not susceptible to detachment and can be applied relatively easily [7, 8]. Deposits applied by welding can be used with a thickness greater than most other techniques, typically in the range of 3 to 10 mm.

Within the techniques of hard facing by welding, the manual hard facing by electric arc is very used and, often, the only possible solution in the restoration of pieces, even when it is recognized as an unproductive process. Generally, the configurations of the pieces or their dimensions do not allow to use another process, with some degree of automation. The need to perform short welds and use electrode oscillation techniques also influences. In addition, the simplicity of the equipment and the possibility of profitably manufacturing a specific consumable, in small batches, for a given application are valued, making it the most economical and versatile method [9, 10].

To achieve the functionality characteristics of the electrodes, they must have a certain coating composition. The coating, in the case of the electrodes destined to the recovery of pieces, must be composed of a matrix and an alloy charge. The coated electrodes are the consumables that allow reaching the highest transfer levels because of the potentialities of the coating in terms of alloy input [11, 12].

Some of these required characteristics of the electrodes may be incompatible and, therefore, compromises and balances between them must be observed when designing the coating.

The chemical composition of the alloy charge significantly affects the chemical composition of the deposited metal and its mechanical properties. The loss of the alloying elements can be replaced by the addition of some ferroalloy. By doing so, the transfer of alloying elements could be greater, that is, the percentage of the element that is transferred from the electrode to the weld metal [13]. The introduction of metallic elements in an alloy based on iron and high carbon content will fulfill two functions [14]: On the one hand, the elements forming carbides participate in the formation of this phase; on the other side, the alloying elements influence the properties of the alloy matrix.

The solid electrodes destined to the recharge, whose nuclei are formed from steel with low carbon content and without alloys, have an alloy charge in the coating, whose function is to transform the core metal into a special alloy [15].

For this purpose, are added special substances and compounds to the coating, whose functions could compete with others designed to guarantee adequate operating properties of the electrode [16]. The way to obtain the combination between these coating compounds is vital to achieve efficiency in the transfer process [17]. In conventional electrodes for hard facing, it is not common to use high alloy cores. In these cases, the codes restrict the current values to avoid the overheating of the core and reduce the values of the caloric contribution in the welding bath.

The homogeneous mixtures of the alloy charge and the electrode coating may not lead to solutions that favor the use of the entire alloy charge of the solid electrodes destined for hard facing.

The homogeneous mixture of the alloy filler with an oxidizing silicone matrix and the use of binders in conventional electrodes for the recharge presuppose a considerable loss of the alloy charge during the transfer, from the coating of the electrodes, to the welding bath. The result of intensive oxidation processes of ferroalloys in the arc column, depending on the affinity of the metal element for the oxygen contained in the materials, which make up the coating, which decreases the percentage of alloy elements that reaches the deposit [18].

Hardfacing electrodes must fulfill their main function: to achieve the incorporation of elements of alloy, which allows reaching the special characteristics to face certain wear mechanism [19].

Established a classification of the electrodes in terms of the constructive structure of the electrode coverings. Thus, classified the electrodes in terms of the thickness of the coating and the structure of the coating. As for the thickness, the coatings are classified as fine, medium, thick and extra-thick [20]; as for the structure of the coatings, the electrodes can be single-coated and double-coated [21]. To this last aspect, given for several years more interest for potential to improve the technological properties of the process [20].

Currently, manufactured double-coated electrodes with great success in several developed countries [22]. It has achieved high stability of the arc and a metallic transfer of fine droplet, from locating the fluorite in the outer layer and the elements of low ionization potential ($CaCO_3$) in the interior.

The use of electrodes with double coating also makes it possible to increase the stability indicators of the arc, when welding with alternating current, using transformers with low vacuum voltages [23]. However, identified the position of the alloy charge to achieve adequate performance in the operational behavior of the electrodes and the transfer of alloying elements to the deposits. Valuations on these aspects, in electrodes with a double coating structure applied in the hard facing, have not found explicitly in the consulted literature.

2. Materials and Methods

2.1 Materials

To obtain the coatings of a double layer electrode it was necessary to prepare two charges of raw materials, one for each layer. One layer, to guarantee the operating parameters of the electrode, constituted by 70% of the dry mass of the commercial composition, manufactured for the coating of a rutile electrode E6012.

Designed another layer (30% of the dry mass) to provide the alloy charge. The proportions of 70 and 30% are assumed, according to recommendations in the literature [22] and seeking to ensure that the stability of the process does not become an independent variable.

Manufactured three types of electrodes with the same chemical composition for the metallic core and the alloy charge (Table 1). Likewise, the same coating was used (Table 2), similar to that of an E6012 electrode [2]. Where: D1 is the first layer diameter, *Dex* is the external diameter and *d* is core diameter.

The coating of the alloy charge for each type of electrode occupied the same cross-sectional area of the coating and therefore the same measurement in the total volume of the coating, in the same way that of E6012 is used. Where: A_1 is alloy charge section area and A_2 is electrode coating E6012 area. The binder used was also common for all electrodes: sodium silicate, with a density of 1.44 to 1.48 g / cm3, occupying between 28% and 30% of the total mass of the coating.

Table 1. Chemical composition of the raw materials used in the preparation of the electrodes

Electrode component		Percent, in mass, of the chemical element in each component of the electrode					
Mn		Cr	C	Si	Ti	Fe	
Wire		0.48	0.11	0.11	0.4	0.002	Balance
Alloy-Charge	Ferro-chrome	0.00	75.00	0.10	2.00	0.00	Balance
	Ferro-chrome-manganese	59.02	19.45	0.11	2.17	0.00	Balance
	Graphite	0.00	0.00	99.50	0.00	0.00	Others

Table 2. Chemical composition of electrode coating E6012

Chem. composition en %	SiO_2	Al_2O_3	TiO_2	NaO	$CaCO_3$	FeMn	$C_6H_{10}O_5$
E6012	16	6	52	2.5	2.5	14	7

For the research, established the formulation of three prototypes of electrodes as a comparative strategy, whose differences were not in their composition, but in the position occupied by the alloy charge and the matrix in the structure of the electrode coating (Figure 1).

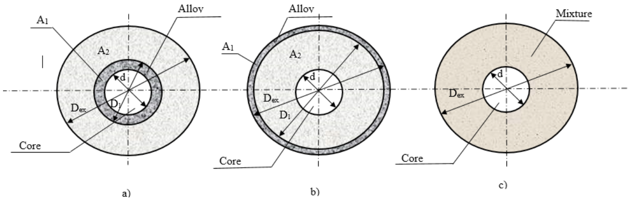

Figure 1. Geometric diagrams of the conformation of the coatings on the electrodes

a) doubly coated (internal alloy charge) b) doubly coated (external alloy charge) c) simply coated(alloy charge homogeneously distributed)

The alloy coating and masses involved in each electrode variant were guaranteed equal, from the consideration of the mass product and the density of each component.

As a result, obtained the dimensions of the different coatings for each developed electrode variant (Table 3).

Table 3. Electrodes dimensions

Electrode type	Diameter (mm)			Weight(*) (g)
	Core (d)	Internal-layer (D_1)	External-layer (D_{ex})	
Internal alloy charge	3.0	4.5	6.5	22.764
External alloy charge	3.0	5.8	6.5	22.766
Simply coated	3.0	-	6.5	22.763

***** Electrode length: 250 mm

2.2 Methods

Established the experimental planning was to satisfy the objective of the work in relation to the evaluation of the effect of the position that occupies the alloy charge(C-Cr-Mn) in the structure of the coating of an electrode for the recharge. The position of the alloy charge in the lining structure was taken as an independent factor

Due to the characteristics of the experiment, it was convenient to use a completely randomized design (CRD) [24, 25].

The set of hypotheses to be tested when applying the ANOVA test to the data, according to the CRD, was [24]:

DOI: https://doi.org/10.30564/jmer.v4i1.2890

Ho: The means of the treatments are the same ($\mu 1 = \mu 2 = \mu 3$)

H1: Some pair of means of the treatments differ ($\mu i \neq \mu j$ for some $i \neq j$; $i = 1, 2, 3$)

We used the Statgraphics Centurion XV software as a tool for the study [26].

Among the dependent factors, the stability of the arc was considered.

The acquisition of data on the electrical behavior allows differentiating the operational electrical stability of homologous electrodes [16], then, it can be used to identify differences between the behaviors of electrodes manufactured with different position of the alloy charge in the structure of the coating during the recharge process.

The use of alternating current allows evaluating the behavior of the electrodes in both polarities. The evaluation of its use, presupposes to estimate with which of the two polarities would behave better, from the point of view of the stability of the arc, in the case that both half cycles of current and voltage are asymmetric.

The installation for the acquisition of the signals was composed by a welding station, which includes the alternating current source, a signal conditioner, a shunt, a computer and a digital oscilloscope Tektronix DPO 3014; the latter captured and saved the data obtained, which were processed with the MatLab software [26]. The alternating current source used was an Airco transformer, 200 A, AC / DC Heliwelder Model: 2A / DDR- AC, maximum vacuum voltage 80 V, 200 A with a duty cycle of 60%. The electrodes used to obtain the deposits were dried before the test, between 90 and 120 ºC, for 2 hours, in a "Conterm" model stove. Carried out the maintenance of the electrodes in a portable thermo (HydroGuard), from Lincoln Electric.

The data collected constituted samples of peak voltages of re-ignition of the arc, welding voltage and maximum current in each half-cycle, at a frequency of 12000 Hz, above 5000, recommended in the specialized literature [16], according to the theorem of Nyquist-Shannon sampling [27].

As a criterion to measure the stability of the arc (Equation 1), the average rate of increase in electrical conductivity in the arc column during the period of re-ignition in the positive half-cycle (B^+) was taken [2]. Which is directly proportional to the average re-ignition peak current (I_r^+) and inversely proportional to the product of the average re-ignition voltage (V_r^+) with the average re-ignition peak time (t_r^+), all measured in the positive half-cycle.

$$B^+ = \frac{I_r^+}{V_r^+ \cdot t_r^+} \cdot 1000 \qquad \text{(Equation 1)}$$

3. Analysis and Discussion

From the census, conditioning, recording and digital processing of the current and voltage signals taken during the operational tests, are constructed the graphs (Figure 2) to compare the performances of the electrodes evaluated. Considering a mean welding time of 40 seconds for each variant, a total of more than 10^6 samples were counted during the study of each electrode, which allowed obtaining the current and voltage oscillograms (Figure 2) and the subsequent analysis of the behavior of the main electrical parameters (voltage, current and re-ignition peak voltage). These readings were sufficient to make the statistical comparisons.

In accordance with the criteria published in the literature [16], robust comparison parameters in the current and voltage oscillograms of the welding arc are recognized at the re-ignition peak voltages, the welding voltages and the maximum current.

The values of the welding current (Table 4) oscillate by more than 1% in the case of the positive half cycle, while approximately 5% in the negative half cycle. This refers to more stability in one cycle than the other, with the negative half cycle being the most suitable for comparing the electrodes, since this is where the greatest differences in their behaviors can be observed.

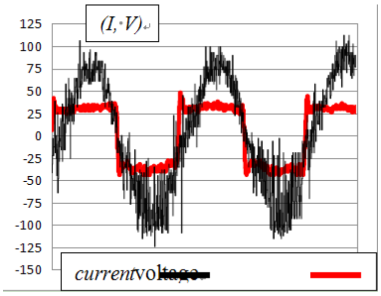

Figure 2a. Fragments of current (I) and voltage (U) oscillograms, obtained during the operational test of the electrodes evaluated (sampling time 0.042 s)
a) Electrode with internal alloy charge

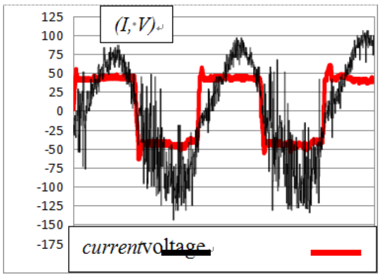

Figure 2b. Fragments of current (I) and voltage (U) oscillograms, obtained during the operational test of the electrodes evaluated (sampling time 0.042 s)
b) Electrode with external alloy charge

DOI: https://doi.org/10.30564/jmer.v4i1.2890

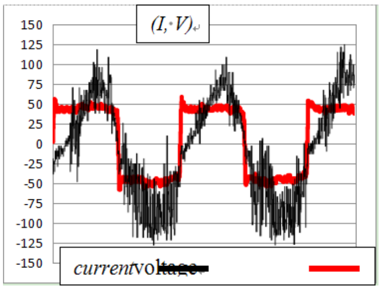

Figure 2c. Fragments of current (I) and voltage (U) oscillograms, obtained during the operational test of the electrodes evaluated (sampling time 0.042 s)
c) Electrode with homogeneous coating

The values of voltage registered for the performance of electrodes with internal alloy charge (32 V and -34 V) present differences of about ten volts with respect to the values obtained for the electrodes with external alloy charge and alloy charge homogeneously distributed (43 V and -46 V). This agrees with the values obtained by Vornovitsky et al. for rutile coating electrodes and alloy core [28].

The voltage value is associated with the magnitude of the arc length: result of the sum of the anodic, cathodic and arc column lengths; the first two are practically constant for the same coating compositions and the same metal core material [29].

Then, in this case, the length of the arc depends on the length of the column, which, in turn, the depth influenced the coating cup. French [30] supports the same criterion. Therefore, the arc length may be influencing the differences (Figure 2) of the voltage values between the electrodes with internal alloy charge (32 V and -34 V) and the electrodes presented by the external alloy charge and homogeneously distributed alloy charge (43 V and -46 V).

Table 4. Electricalindicators. Averagevalues

Parameters	**Units**	**Position of the alloy charge**		
Average maximum current		**inter-nal**	**external**	**homogeneusus**
Maximum average current (Imax+)	Ampere	112.4	113.1	114.3
Maximum average current (Imax-)	Ampere	-138.3	-147.7	-150.5
Average current of re-ignition peak (Ir+)	Ampere	9.67	11.33	11.67
Average re-ignition voltage (Vr+)	Volt	42.7	53.1	53.6
Average re-ignition voltage (Vr-)	Volt	-43.6	-52.5	-50.9
Average welding voltage (Vs+)	Volt	32.7	43.9	43.1
Average welding voltage (Vs-)	Volt	-34.1	-46.3	-42.1
Average re-start peak time (tr+)	Second^{-3}	0.76	0.86	0.75

(+) in the positive half-cycle; (-) in the negative half cycle.

The thermo-physical properties in a zone of the coating, composed of silicates, are different to that composed of metallic components, due to the thermal conductivity of the materials that compose it. In electrodes with an internal alloy charge, which has greater thermal and electrical conductivity, than the rest of the coating, it will melt first (because of the aforementioned and because it is closer to the area of higher arc temperature). Then, practically in unison with the metallic core and the ordinary coating layer, it will then melt. This process induces the participation of a greater number of conductive elements in the column, to the process of conduction in the arc and, therefore, to the reduction of its voltage, being able to generate a smaller coating cup. When the alloy layer is located at the periphery of the coating (externally), the ordinary coating layer functions as a physical barrier. This leads to the outer alloy layer being less exposed to high arc temperatures. Then, the position of the alloy charge in the electrode coating structure produces differences in arc conductivity and is exposed to the different melting temperatures.

All the previous analyzes have no meaning if they do not contribute to differentiating the stability of the welding process. Therefore, the stability of the arc is determined B^+ (Equation1), from the voltage, current and re-ignition time values obtained, determining the value of B^+ (Figure 3) for each variant studied.

The values of B^+ indicate satisfactory stability values for all variants, being slightly better for the variants with internal alloy charge (371.21 Ω-1 · s-1) and homogeneous (309.39 Ω-1 · s-1)). The values of B^+ obtained in the work are higher than those obtained by the aforementioned authors [31] and since the coatings used have SiO_2, TiO_2 and graphite in sufficient quantities (Table 1), they could be responsible for this behavior.

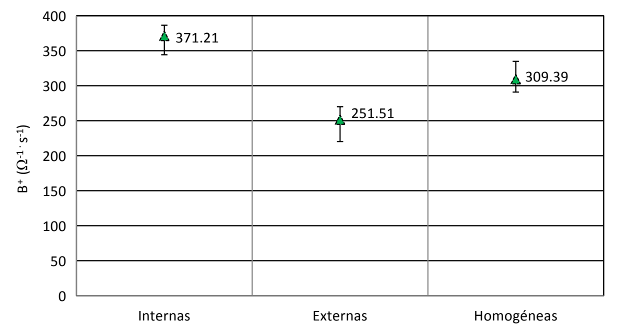

Figure3. Arc stability indicator B^+

The ionization potential and the inverted energy in the dissociation and ionization processes, which make up the column of the arc, determine the stable functioning of the arc [14]. It is argued by Pokhodnya [20] that TiO_2 has an effect of stabilizing the arc, reaching values of 400 Ω^{-1} ·

s^{-1} for 100% of rutile in the coating. In addition, the presence of elements with lower ionization potential (sodium present in the binder), considerably increases the stability of the arc [2]. Both aspects guarantee an electrical stability (B^+) suitable for the realization of the process; however, it is more effective in the case of the electrode with the internal alloy charge, due to its more active participation within the arc column.

4. Conclusions

The tests for the determination of the electrical stability make it possible to establish criteria that allow differentiating the operative behavior of the electrodes evaluated with different position of the alloy charge in the coating structure.

The relative high percentage of elements with low ionization potential and metallic elements, which characterizes the alloy charge, produces differences in the behavior of the average rate of increase in electrical conductivity in the arc column during the re-ignition period (B^+), inversely proportional to the value of the average re-ignition voltage (Vr^+). Therefore, the position of the alloy charge in the coating structure defines the behavior of the electrical stability of the process, resulting in the best performance ($B^+ = 371.21\ \Omega^{-1} \cdot s^{-1}$) in the electrode with internal alloy charge.

The results of the experiments carried out establish that the relative position of the alloy charge C-Cr-Mn in the coating structure of rutile electrodes (E6012) significantly influences the operational behavior (stability of the arc) in the hardfacing process.

References

[1] Surian, E.S., Consumibles para soldadura por arco eléctrico: algunos desarrollos recientes. Soldag. Insp. São Paulo, 2013. 18(01): p. 077-089.

[2] De Rissone, N.M.R., et al., ANSI/AWS A5.1- 91 E6013 rutile electrodes: The effect of calcite. Welding Journal, 2002. Supplement p. 112-124.

[3] Yunus, M., M.S. Alsoufi, and M. Irfan, APPLICATION OF QC TOOLS FOR CONTINUOUS IMPROVEMENT IN AN EXPENSIVE SEAT HARDFACING PROCESS USING TIG WELDING. International Journal for Quality Research, 2016. 10(3).

[4] Colectivo de autores, Estudio comparativo de los parámetros de consumo y geometría de los depósitos de electrodos tubulares revestidos para recargue, Universidad Central ¨Marta Abreu¨ de Las Villas, Cuba. Universidad Federal de Uberlândia, Brasil. 2007.

[5] Pérez-Cepeda, J., La influencia de la microestructura en el comportamiento al desgaste abrasivo evaluado bajo norma astm g 65 de depósitos de soldadura antidesgaste aplicados sobre sustratos de acero de baja aleación y bajo carbono. Tesis Magister en Ingeniería, in Facultad de Ingeniería, Departamento de Ingeniería Mecánica y Mecatrónica. 2011, Universidad Nacional de Colombia: Bogotá D.C p 109.

[6] Herrera-Artiles, A., Sistema alambre - fundente para la recuperación de árboles cigüeñales y otras piezas tipo eje mediante soldadura por arco sumergido. Tesis doctoral. Facultad de Ingenieria Mecánica. Universidad Central de las Villas. Santa Clara. 2006.

[7] Yildizli, K., M. Eroglu, and M.B. Karamis, Erosive Wear Behaviour of Hardfacing Austenitic Manganese Deposit Tribology in industry, 2005. 27(3&4): p. 15-21.

[8] Rude, A. and M.D. Pimpalgaonkar, Optimization Of Process Parameter In Hardfacing By Shield Metal Arc Welding (SMAW). International Research Journal of Engineering and Techonology, 2018. 5(8): p. 232-236.

[9] Walh, W. Trend to hardfacing. Stuttgart. Consultado 15/10/2015. Disponible en: http://www.engineers.org.il/_Uploads/1638drwahl0206.pdf.

[10] Bracarense, A.Q. and S. Liu, Chemical composition variations in shield metal arc welding. Welding journal, 1993. Welding research supplement(72): p. 529-535.

[11] Hardfacing. Welding consumables. Afrox product reference manual. Consultado 09/10/2015. Disponible en: http://www.afrox.co.za/en/legacy/attachment?files=tcm:g266-154582,tcm:266-154582,tcm:66-154582. p. 63.

[12] Cruz-Crespo, A., R.F. Fuentes, and A. Scotti, The influence of calcite, fluorite, and rutile on the fusion-related behavior of metal cored coated electrodes for hardfacing. Journal of Materials Engineering and Performance, 2010. 19(5): p. 685-692.

[13] Linnert, G.E., Welding Metallurgy, Vol. 1,American Welding Society, Miami, FL 1994(Chapter 9, p. 820).

[14] Livshits, L.C. and A.H. Jakimov, Ciencia de los metales para soldadura y tratamiento térmico de las uniones soldadas (En ruso), ed. Mashinostraenie. 1989, Moscu. p. 336.

[15] González Cabrera, O., C.R. Gómez Pérez, and U.B. Del Pino Paz, Methodology for the Selection of the Best Variant Between Double Coated Electrodes for Hardfacing. TecnoLógicas, 2020. 23(49): p. 53-62.

[16] García-Rodríguez, A., Evaluación de la estabilidad eléctrica específica de electrodos revestidos. Tesis doctoral. Centro de Investigaciones de Soldadura. Universidad Central "Marta Abreu" de Las Villas.

2010. p. 159.

[17] Queiroz Bracarense, A., et al., Desarrollo de electrodos tubulares revestidos para la soldadura subacuática mojada. Revista Técnica de la Facultad de Ingeniería Universidad del Zulia, 2009. 32(2): p. 89-97.

[18] González-Cabrera, O., Gómez-Pérez, Carlos-René; Quintana-Puchol, Rafael; Perdomo-González, Lorenzo; Miguel-Oria, Jorge-Víctor; López-Fontanills, Roney-Lázaro., Alternativa de doble recubrimiento para electrodo destinado al proceso de relleno manual con arco eléctrico. Rev. Ingeniería Mecánica, 2014. 17(3): p. 245-254.

[19] Repair and maintenance Welding handbook, in Repair and maintenance consumables. 2013, ESAB AB: Goteborg SWEDEN. p. 130.

[20] Pokhodnya, I.K., et al., Metallurgy of arc welding. Riecansky Science Publishing CO. London. p. 246. 1995.

[21] The Welding Handbook. Edition 11 Revision 0, ed. W.M. Services. 2015, Lysaker, Norway. p. 556. Edition 11 Revision 0, ed. W.M. Services. 2015.

[22] Marchenko, A.E., N.V. Skorina, and V.P. Kostyuchenko, State of the art of development and manufacture of low hydrogen electrodes whit double-layer coating in the CIS countries. The Paton Welding journal. PWI, International Association «Welding», 2011. 01: p. 41-44.

[23] Baach, H., (1980) Possibilities of new achievements to effect the welding-technological properties of coated electrodes. In:Proc. of Symposium on Welding Industry (Oerlikon, Switzerland). Kiev, 1-10.

[24] Díaz-Rosell, F.A., Diseño Estadístico de Experimentos. Tesis de grado, in Facultad Matemática, Física y Computación. 2006, Universidad Central "Marta Abreu" de Las Villas: Santa Clara.

[25] Diseño de Experimentos (DDE) – Diseños de un Solo Factor Categórico. Diseño Completamente al Azar (DCA) STATGRAPHICS© 2006. por StatPoint, Inc. Consultado: 9/14/2014. Disponible en: http://www.statgraphics.net/wp-content/uploads/2011/12/tutoriales/DDE%20-%20Disenos%20de%20un%20Solo%20Factor%20Categorico.pdf.

[26] STATPOINT, I., Manual de usuario. STATGRAPHICS® Centurion XV. 2006.

[27] Oppenheim AV, Schafer RW. Discrete- time signal processing. Prentice- Hall; 1989. p. 870.

[28] Vornovitsky, I.N., et al., Technological peculiarities of high-alloy steel welding by electrodes with rutile coating. Paton Welding journal, 2005. 2: p. 46-47.

[29] Egerland, S., A contribution to arc length discussion. Soldagem & Inspeção, 2015. 20(3): p. 367-380.

[30] French, I.E., Effects of electrode extension on deposit characteristics and metal transfer of E70T-4 electrodes Supplement To The Welding Journal, 1984. June: p. 167-172.

[31] Makarenko, V.D. and C.P. Shatilo, Stability of arcing in welding with calcium fluoride electrodes. Welding International, 1990. 4(12): p. 988-989.

DOI: https://doi.org/10.30564/jmer.v4i1.2890

BILINGUAL PUBLISHING CO.
Pioneer of Global Academics Since 1984

Journal of Mechanical Engineering Research
http://ojs.bilpublishing.com/index.php/jmer

ARTICLE

Evaluation of Vibration Amplitude Stepping and Welding Performance of 20 kHz and 40 kHz Ultrasonic Power of Metal Welding

Ziad Shakeeb Al Sarraf* Ahmed Fattah Ahmed Khalid Elias Hammo

Department of Mechanical Engineering, University of Mosul, Mosul, Iraq

ARTICLE INFO

Article history
Received: 5 March 2021
Accepted: 13 April 2021
Published Online: 16 April 2021

Keywords:
Ultrasonic welding
Horn design
Vibration amplitude
Stepping amplitude
Welding performance

ABSTRACT

Today ultrasonic power technique is consider a mandatory technique which is always entered in many processes such as in metal and plastic welding to overcomes many issues, with aided of applying force (pressure) and supplied high frequency vibration, a solid-state weld can be generated by ultrasonic metal welding technique. That gives a technique the ability to join not only a small component, whereas also to join thicker specimens, which depends on a proper control of matching welding conditions. Therefore a welding performance can be studied and compared after designed welding horn to resonance at frequencies of 20 kHz and 40 kHz. The analyses of the designed horn are completed through use a vibration mathematical expressions, modal and harmonic analyses to ensure the weldability due to applying ultrasonic power to the working area and also to compare the performance of joint at using two resonance frequencies of 20 kHz and 40 kHz. The dimensions of the horns were determined to match the selected resonance frequencies, which the lengths were calculated as 132 mm and 66 mm respectively. The analysis of the exciting model indicates that the axial vibration modes of 19,584 Hz and 39,794 Hz are obtained in 10th mode, while the two frequency values are recorded 19,600 Hz and 39,800 Hz from the frequency response of the two horns. The weld strength between Al and Cu specimens with a thickness 0.5 mm was evaluated using a tensile test, which the analyses were obtained under using different welding pressure and varied amplitudes. The results were recorded within exciting a horn with two different resonance frequencies, show the enhancement of weld strength and quality through control of stepping amplitude, the enhancement means obtain good strength of the weld, reduce sticking horn to specimen, and lower specimen marking.

1. Introduction

Ultrasonic welding is a technique normally depends on a solid-state bonding process in which the materials are completely joint through applying high frequency in form of shear vibration to create scrubbing between intimate surfaces, and the bonding subjected to force or pressure to confirm bond. The high vibration generated will help to reform the intimate surfaces by vibration deforms and flatten surfaces, removing asperities, oxides and contaminants, and allow for increasing contact area of the weldment specimens [1],[2], this allow the technique

---

**Corresponding Author:*
Ziad Shakeeb Al Sarraf,
Department of Mechanical Engineering, University of Mosul, Mosul, Iraq;
Email: ziadalsarraf@uomosul.edu.iq

DOI: https://doi.org/10.30564/jmer.v4i1.2940

to be applicable on various thinner and thicker materials [3]. Ultrasonic welding technique strongly entered in industrial and manufacturing fields to join materials with good strong and high precision [2]. Furthermore, this technique does not require any adding of filler or solder, which put this type of welding technique to be more suitable for environment specially in reducing carbon emission and controlling of energy conservation environmentally and economically [4]. The main components of an ultrasonic welding system are power supply to generate power, transducer or converter to provide vibration with specific amplitude, booster to raise displacement amplitude and horn to maximize the amplitude and to work. Also, other components such as the anvil for clamp specimens during welding and fixtures, shown in Figure 1. The horn vibrate with different vibration modes, but the tuning is focused on longitudinal mode to ensure that the horn excited at required dynamic characteristics and subsequently effect on strength and quality of weld. The mechanism of the technique is to convert 50 or 60 Hz alternating current into dynamical energy of 20 kHz or 40 kHz. An optional booster is used to raise the limited amplitude of transducer and also enclosed the welding system at nodal zone and the horn transmits the high vibrational motion through carrying ultrasonic energy to the weld materials. Sufficient amount of receiving ultrasonic energy by welded parts depend on high diffusion of material molecular at intimate surfaces [1]. Although many studies have been conducted on ultrasonic welding, using different welding frequencies, various experiments and weldability, but most of these studies pay less attention to examining welding performance between two different horns. In addition, the lack of using controls amplitude stepping for most of previous studies were issued. Therefore, it is required to examine the operating frequency of the horn to improve the performance of the weld and to enhance strength of the various bonding metals. The presented work shows a study of welding performance for join materials by ultrasonic welding technique through improve both weld strength and quality. A numerical design by finite element analysis with ANSYS code and subsequent completing experiments of an integrated welding system with exciting horn at 20 kHz and 40 kHz help to investigate the performance of weld at contact surfaces, and then to allow for study the effect of main welding parameters on welds. The weld strength is characterised experimentally in terms of the results of repeated tensile shear tests. The ability to use amplitude stepping profile is to obtain good weld strength with reasonable quality. Also, to solve several issues such as sticking horn/specimen and part marking.

2. Numerical Design of the Exciting Ultrasonic Horns

A finite element method with code ANSYS is efficiently performed help for design the main components of ultrasonic device (i.e. Horn) , which horn design must has compatibility to the requirement of high amplification and moderate clamping force in order to achieve good welding condition of specimens [5]. Vibrational characteristics such as, resonant frequency of excitation, separation of frequency, amplification of vibration displacement, uniformity of amplitude at horn tip surface, and the distribution of stresses concentration, should be carefully examined during design horn.

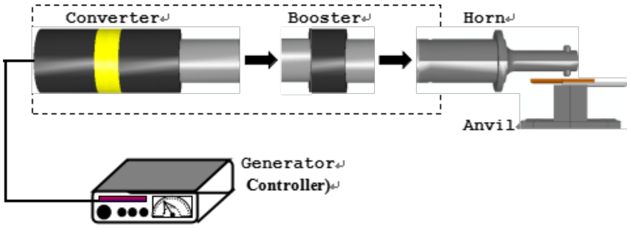

Figure 1. Main components of ultrasonic welding system

The steel is chosen as a selected material for the designing horns, because it has good acoustic properties and suitable to resist against wear. Further with low cost, the steel has good machining material and easy formation to re-shape in different forms. The selection of material depends on the type of weld, properties of weldment such as strength and hardness. It is mentioned here, that the welding member should have material harder than the material of the horn, as this recommended in welding process. Different horn profile can be designed for ultrasonic applications such as exponential, step, conical, catenoidal … etc, which the type of profile indicates the amount of amplification ratio for the horn design. High amplitude amplification is generally recommended with step profile of the horn; however unfavourable stresses should be avoided at working area as these stresses increases due to increase in amplification ratio relative to the radial change in horn diameter [8], but the stresses can be shifted back due to make some modification in the horn profile. In designing a horn, the first step is to determine a length of the horn by using a mathematical expression. Then, the horn length was identified based on relationship between wave length and resonant length. The horn length was roughly determined, and sequentially determined the shape, cross section and dimensions according to the numerical values of mode shape and analyses of natural frequency. It was noted here, that some errors were recorded by theoretical analysis of the horn. After checking all requirements of the horn design, the information of the sketch horn with

DOI: https://doi.org/10.30564/jmer.v4i1.2940

its specification is entered as an input data to the CNC program to get the final shape of fabricated horn. The final shapes of the two dimensional sketches of two frequencies (20 kHz and 40 kHz) are shown as in Figure 2. Table 1 shows the mechanical properties of the horn material (steel alloy) for the finite element analysis of both frequencies.

Table 1. Properties of the horns material

Horn frequency (kHz)	Poisson's effect (-)	Physical density (kg/m^3)	Young's modulus (GPa)
20	0.33	7810	210
40	0.33	7850	207

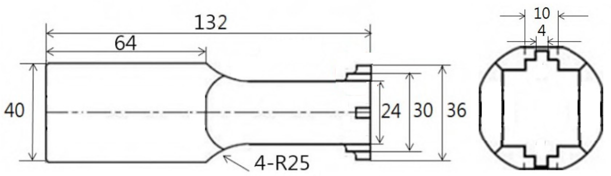

Figure 2(a). 20 kHz two dimensional sketch horn

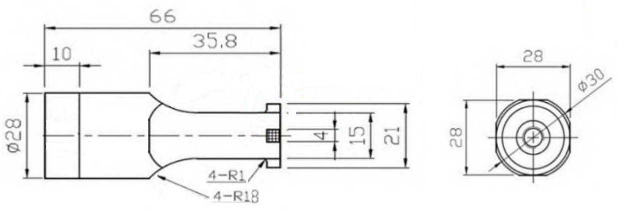

Figure 2(b). 40 kHz two dimensional sketch horn

3. Data Extraction from the Vibration Analysis of the Horns

Finite element analysis is automatically performed through setting the shape and a number of meshes for modelling and analyzing horns. The models were built through sketch the horn and define material properties then assignment the part and apply proper mesh before set boundary conditions, after that the horn restraint through connecting it with bolt, and specified the exciting movement to allow for vibrating horn axially. A high precision CNC machine is performed to design and manufacturing horns. The machine program is set based on the characteristics of the vibrational analysis of selected horn. The analyses of the vibration responses for the designed horns are shown in Figure 3, which the value of the natural frequency of 20 kHz horn is recorded to 19.895 Hz very close to 20 kHz. The frequency response of the horn was calculated at the 9th mode which picks up at the tip of the horn to ensure getting high amplitude. Whereas the vibrational response of 40 kHz horn is recorded 39.654 Hz also close to 40 kHz, which the frequency response is obtained at the 9th mode and through getting high amplitude at horn tip. The analyses of the vibration response for the exciting horn are carried out within frequency range varied from (10-30) kHz and the excitation is collected at the horn surface (horn tip). The results of analysis show an acceptable close to the numerical result of 19.980 Hz. In addition, the harmonic response was also determined at the 40 kHz horn tip, which the data were determined within the range of (30-50) kHz. Similar with the 20 kHz horn, the frequency response of 40 kHz is determined at the output of the horn, which has a value of 39.654 that is close to the result of predicted value. Figure 4 (a) and (b) plots the results of vibration response of the horn at 20 kHz and 40 kHz respectively. The analysis of simulation models shows highest value of amplitude pointed at horn tip, which the horn has good gain in providing displacement amplitude, and the longitudinal mode of vibration for the exciting horn seems to be very close to the result obtained from simulation models. The horn gain was also calculated by dividing the output amplitude / input amplitude of the horn, which the vibration amplitude recorded (17.2 micron), with horn gain 5.5 for the 20 kHz horn, and (26.0 micron), with the horn gain 4.0 for the 40 kHz respectively. However, gain may drop down due to increase coupling between vibration modes, motion distortion and loss in energy which affect on operational processes quantity and quality [8].

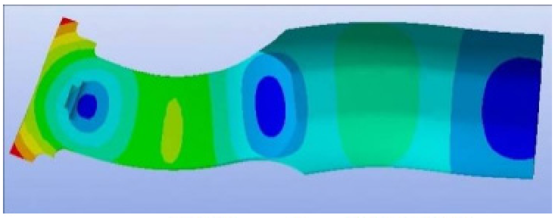

(a) 8th mode – 17.902 kHz

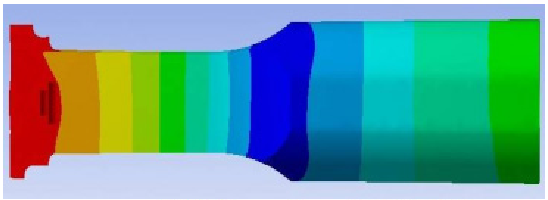

(b) 9th mode – 19.895 kHz

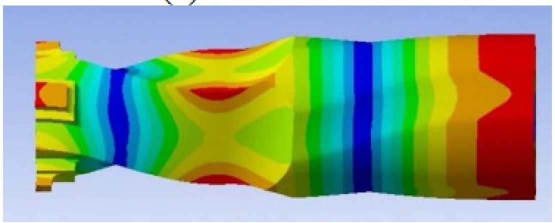

(c) 11th mode – 27.266 kHz

Figure 3(a). Prediction the separation frequency modes at 20 kHz

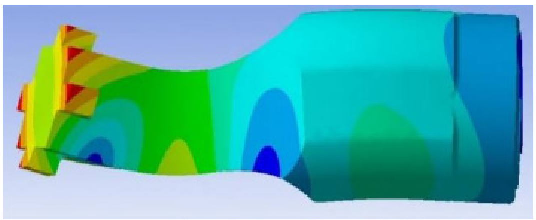

(a) 8th mode – 38.222 kHz

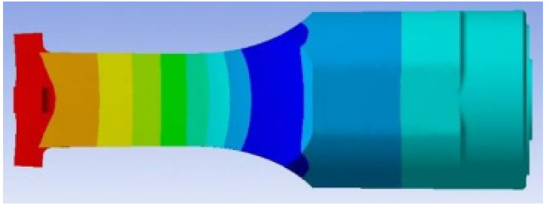

(b) 9th mode – 39.654 kHz

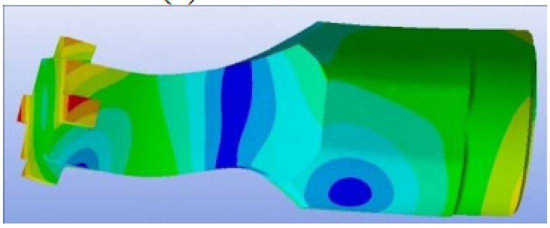

(c) 11th mode – 48.520 kHz

Figure 3(b). Prediction the separation frequency modes at 40 kHz

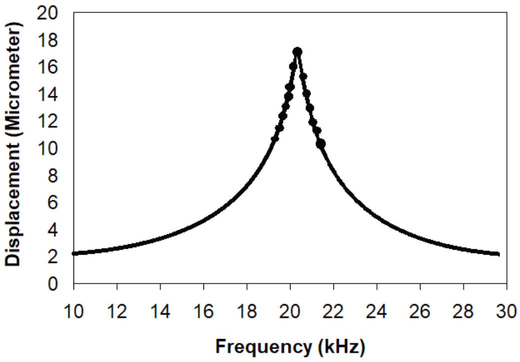

Figure 4(a). Vibration response analysis of the designed horns at 20 kHz

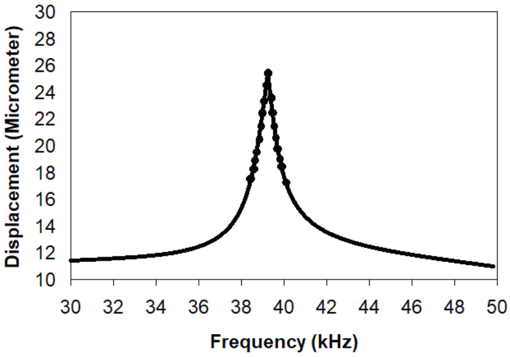

Figure 4(b). Vibration response analysis of the designed horns at 40 kHz

4. Welding System and Their Parameters

4.1 Set up of Welding Process

In order to joint specimens, welding system should be built, assembled and to work. The horn which is considered the main component of the welding system was designed precisely and accurately to produce weld according to the type and requirements of materials to be welded. First, the horn was directly connected to the transducer (sometimes adding booster between horn and transducer), which form welding stack. The transducer linked to the power supply (generator, type Sonic) to receive an alternative current from the electric main point. With 1 kW maximum capacity of ultrasonic generator the designed horns were excited at operating frequencies to provide sufficient mechanical vibration needed for welding. A tensile machine is performed to hold welding stack and to support welding specimens being sit on stationary anvil. Also, tensile machine has ability to control and measure the force applying over weldment during process, and to record the value of force by the 2.0 kN machine load cell. A computer program that equipped by tensile machine is saved the amount forces applied against the time. Horn tip is designed in the form of flatten with knurled surface to help for contact with upper specimen and avoid it from slippage during vibration, while the lower specimen is strongly held by anvil (shown in Figure 1). The aluminium and copper specimens were cut and prepared according to the ASTM and BSI Standard codes [6], [7]. Specimens dimension was set to be 50 x 10 mm for all sheets that having thickness 0.5 mm. 10 mm was set for overlap specimens to match with the dimension of horn tip, as shown in Figure 5. During the test of welded specimens' strength, the bending effect on specimens was observed and that resulted from error in measuring strength. Therefore, to avoid bend a dummy plates were added. Several trials were carried out on different welding conditions, each trial was repeated five or six times prior to get results, then the results were averaged and the standard deviation was extracted for each trial. The trials were arranged in order of welding (Al-Al) specimens and (Cu-Cu) specimens. A number of failed trials were excluded from results, because those specimens that are sticking with horn or either those trials that required more power or applied force to confirm joints. In experimental trials, input welding parameters were set to ensure good joint and to evaluate the weldability of the weld specimens, these parameters are process time, applying force and vibration amplitude.

DOI: https://doi.org/10.30564/jmer.v4i1.2940

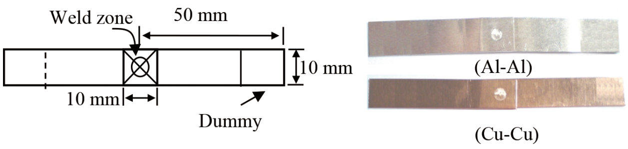

Figure 5. Specimen layout and welded coupons with welding area

4.2 Stepped Amplitude

In ultrasonic processes, generally ultrasonic amplitude apply to the process has a constant value, which its value can be pre set to higher or lower value depends on the specification of the welding system. However, an alternative technique which is presented in this work is to apply amplitude stepping. The stepping here allows the weld to be done by controlling amplitude between two different values. The digital screen of ultrasonic generator with controlling knobs allow to trigger for the transitions of the setting amplitude values, which pre setting can be made by either time period of weld process or change the energy level or power [10]. The procedure for applying stepping amplitude begin with pre set high amplitude value as this value is required to provide sufficient joints for overlapping specimens and to create a solid-state form of welding. Then, the amplitude is suddenly lowered to minimize the frictional heat between intimate surfaces and allow for high interlock atoms of materials diffusion. It was noted here, that stepping process made the samples soft, less damage and lower sticking to the horn tip. A series of experiments have been conducted on 20 kHz and 40 kHz design horns using stepped amplitude to investigate welding performance and to ensure obtained good enhancement for the both strength and quality of joining parts.

4.3 The Influence of Joining Metals by Using Constant and Stepped Amplitude

The weldability of the 20 kHz and 40 kHz designed horns was successfully done to evaluate the weld processes through which the strength between specimens were compared and analysed. Figure 6 (a) and (b) plots a relationship between the strength of the de-bonded specimens against the values of applying force, which the relations were carried out on using 0.5 mm specimens thickness that welded ultrasonically at 20 kHz and 40 kHz respectively. The welding processes were carried out through applying different constant and stepped vibrational amplitudes. For each input parameters, five tests were done, then the average values were determined with error bars, so the standard deviation indicates the variation of strength against applying force. It was noted that the welding strength is increased due to increases in clamping force and for the process time up to one second, but it was observed that excessive force may produce high friction, more heat and then suppress the relative motion between surfaces, which in turn lower weld strength [9]. Overall, the strength of weld is proportional to the time under the influence of applying clamping force, which lower values of strength were recorded with 40 kHz than 20 kHz under the common value of selecting amplitude. The reason for that either due to friction heat generated between joining specimens is concentrated at tip of the horn, also the diffusion at intimate surfaces of selected materials which is facilitated at 20 kHz compared with 40 kHz. For the welding of Al-Al specimens, the maximum strength recorded is 880 N at 20 kHz under clamping force of 680 N and vibration amplitude 17 μm, while at 40 kHz, the maximum strength was recorded 820 N under clamping force of 700 N and vibration amplitude 17 μm. Figure 6 confirms that the weld strength increased with increasing of amplitude to 26 μm. The welding strength versus clamping force tests were determined with welding of Cu-Cu specimens, which the maximum strength of 20 kHz horn was recorded 790 N at clamping force 700 N and amplitude 17 μm, and the maximum strength of 40 kHz horn was recorded 770 N at clamping force 750 N and amplitude 17 μm. Similar to the weld Al specimens, the weld strength of joining Cu-Cu specimens increased with increasing amplitude to 26 μm, but the overall that the strength of Cu stay below of Al specimens. No evidence indicates that the strength of weld increases due to increase the value of clamping force for welding material specimens. In case of setting amplitude 26 μm, despite resulting high strength, it also leads to increase in standard deviation beside leave a noticeable mark on joint specimens. During experiment, part of trials was failed due to sticking of horn tip/upper specimen. However, sticking parts become more prevalent on specimens when the welded specimens subjected to a value of clamping force above 600 N, but this result to lower in weld strength despite using constant and stepped amplitudes. Further, it was shown that the strength is significantly affected by the material properties such as hardness and roughness, as higher strength values were recorded with aluminium specimens than copper specimens.

In Figure 6, the influence of applying stepping amplitude technique is shown through indicate the weld strength values taken at different clamping forces. The advantages of changing the amplitude from higher value (26 μm) to lower value (17 μm) were clearly seen in Figure 6, through reducing the size of error bars and lower in standard deviations, and in contrast increase in weld strength, but during examine the weld strength, aluminium specimens show slightly higher values of strength compared with copper specimens under using identical parameters. Finally, it was observed that applying the stepped amplitude will improve weld consistency and reduce other issues such as sticking, part marking, tool fracture and glowering. Further, the use of stepping amplitude may enhance the quality of welding and provide proper strength for joining materials.

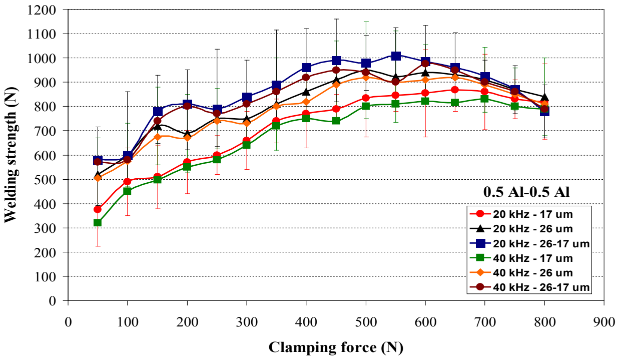

Figure 6(a). Variations of weld strength vs. clamping force for joined specimens: Al-Al for process conditions and frequency of designed horns at 20 kHz and 40 kHz

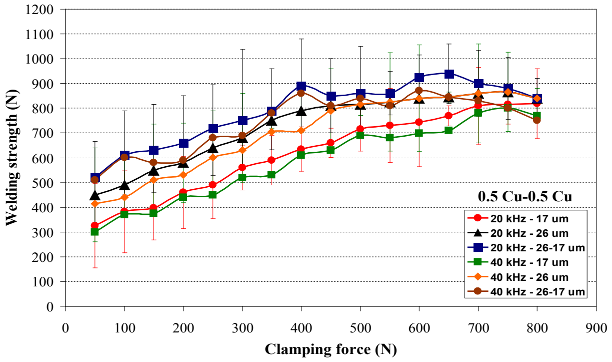

Figure 6(b). Variations of weld strength vs. clamping force for joined specimens: Cu-Cu for process conditions and frequency of designed horns at 20 kHz and 40 kHz

5. Conclusions

This work presents a design, simulation and fabrication of an ultrasonic welding system in order to study and evaluate the weldability of joined specimens through using two different horns that are excited by 20 kHz and 40 kHz. Finite element analysis is performed successfully to examine frequency response through analyses of both modal and harmonic response. The welding input parameters such as force, amplitude and specimens arrangement have a significant effect on the strength of weld, which higher strength observed for those specimens of weld aluminium to aluminium compared with slightly lower strength measured for welding copper to copper specimens. For all trials the weld strength exhibits high values due to increase in clamping force, but excess in applying force above 600 N will result to deteriorate and drop in weld strength. An evaluation of weld strength is carried out through using three amplitude values, starting from 17 micron to 26 micron for normal constant amplitude, then a comparison is done for apply stepping amplitude process of previous two amplitude values (26-17), to improve weld strength, reduce error bars and lower standard deviation. In addition, the stepping process allows for reducing specimen adhesion to the horn and lower specimen marks. According to the change in welding condition, the overall tendency of weld strength increases with the increase in clamping force during process time up to one second. The overall tendency of evaluating weldability shows that the weld strength significantly affected by welding parameters such as time and amplitude, and it have direct proportional with these two parameters, but the strength does increase due to increase in clamping force. The study confirmed that lower weld strength of joint specimens was determined by 40 kHz compared with 20 kHz, even when using the same vibration amplitude or applying stepping amplitude. The reason is related to the amount of friction heat concentration at joint, and another reason is the facility of diffusion at weld interface for the both selecting materials, means that aluminium exhibit more to diffuse than copper for the two design operating frequencies.

Acknowledgment

The authors would like to express their thanks to the dynamic and vibration laboratories in department of mechanical engineering for their funding, the University of Mosul for the sponsorship under its research and development program, also for supporting of the research.

References

[1] E. deVries, 2004, Mechanics and Mechanisms of Ultrasonic Metal Welding, PhD Thesis Ohio State University.

[2] K. Graff, 2005, Ultrasonic Metal Welding, in New Developmets in Advanced Welding Cambridge, 241-269.

[3] M. Bloss and K. Graff, 2009, Ultrasonic Metal Welding of Advanced Alloys: The Weldability of Stainless Steel, Titanium, and Nickel-Based Superalloys, Trends in Welding Research Proceedings of the 8th International conference, ASM International.

[4] S. Kim, H. Sung, E. Kim and D. Park, 2010, Vibration Analysis of Ultrasonic Metal Welding Horn For Optimal Design, Proceedings of the International Conference on Mechanical, Industrial, and Manufac-

DOI: https://doi.org/10.30564/jmer.v4i1.2940

turing Technologies, Sanya China.

[5] Ziad Sh. Al Sarraf, 2012, Enhancement Weld Strength Due to the Control of Amplitude Profiling For Joining Metals by Ultrasonic, Unpublished.

[6] ASTM International Codes, 2009, Standard Test Methods for Tension Testing of Metallic Materials, 1-24.

[7] British Standard Codes, 2009, Test Pieces and Test Methods for Metallic Materials for Aircraft, Metric units 1-7.

[8] Ziad Sh. Al Sarraf, Majid M. Chilmeran, 2018, Design and Analysis of Slotted Block Horn Used For Ultrasonic Power Applications. Journal of Southwest JIAOTONG University, Vol , No.
DOI: 10. 3969 /j, ISSN. 0258-2724.

[9] M. Hiraishi and T. Watanabe, 2003, Improvement of Ultrasonic Weld Strength for Al-Mg Alloy by Adhesion of Alcohol - Ultrasonic Welding of Al-Mg Alloy, Quarterly Journal of the Japan Welding Society, 21(2), 295-301.

[10] M. Baboi and D. Grewell, Evaluation of Amplitude Stepping in Ultrasonic Welding, Welding Journal, Sponsored by the American Welding Society and the Welding Research Council, 2010.

BILINGUAL
PUBLISHING CO.
Pioneer of Global Academics Since 1984

Tel:+65 65881289
E-mail:contact@bilpublishing.com
Website:www.bilpublishing.com

ISSN 2630-4945
01
9 772630 494214